



Centrality and transverse momentum dependence of inclusive J/ψ production at midrapidity in Pb–Pb collisions at $\sqrt{s_{NN}} = 5.02$ TeV

ALICE Collaboration*



ARTICLE INFO

Article history:

Received 16 November 2019
 Received in revised form 8 February 2020
 Accepted 15 April 2020
 Available online 21 April 2020
 Editor: W.-D. Schlatter

ABSTRACT

The inclusive J/ψ meson production in Pb–Pb collisions at a center-of-mass energy per nucleon–nucleon collision of $\sqrt{s_{NN}} = 5.02$ TeV at midrapidity ($|y| < 0.9$) is reported by the ALICE Collaboration. The measurements are performed in the dielectron decay channel, as a function of event centrality and J/ψ transverse momentum p_T , down to $p_T = 0$. The J/ψ mean transverse momentum $\langle p_T \rangle$ and r_{AA} ratio, defined as $\langle p_T^2 \rangle_{PbPb} / \langle p_T^2 \rangle_{pp}$, are evaluated. Both observables show a centrality dependence decreasing towards central (head-on) collisions. The J/ψ nuclear modification factor R_{AA} exhibits a strong p_T dependence with a large suppression at high p_T and an increase to unity for decreasing p_T . When integrating over the measured momentum range $p_T < 10$ GeV/c, the J/ψ R_{AA} shows a weak centrality dependence. Each measurement is compared with results at lower center-of-mass energies and with ALICE measurements at forward rapidity, as well as to theory calculations. All reported features of the J/ψ production at low p_T are consistent with a dominant contribution to the J/ψ yield originating from charm quark (re)combination.

© 2020 European Organization for Nuclear Research. Published by Elsevier B.V. This is an open access article under the CC BY license (<http://creativecommons.org/licenses/by/4.0/>). Funded by SCOAP³.

1. Introduction

The Quark–Gluon Plasma (QGP) is a state of strongly-interacting matter characterized by quark and gluon degrees of freedom predicted by Quantum Chromodynamics (QCD) to exist at high temperature and energy density [1,2]. Such conditions are realized during the initial hot and dense stages of ultra-relativistic heavy-ion collisions. The medium produced in these collisions has a short lifetime, which is of the order of 10 fm/c at the energies reached at the CERN Large Hadron Collider (LHC), see e.g. [3].

Due to their large masses, charm and beauty quarks are produced in hard partonic scatterings occurring during the early stage of the collision and therefore experience the full evolution of the medium. Charmonia, i.e. the bound states of charm and anti-charm quarks, are of particular interest for the understanding of the QGP, see e.g. [4,5]. In the framework of color-screening models, the suppression of the charmonium state J/ψ is an unambiguous signature of the QGP [6,7]. The high density of color charges prevents charm and anti-charm quarks from forming bound states. Therefore, the J/ψ yield is expected to be suppressed compared to probes unaffected by the hot and dense medium or from expectations of the incoherent superposition of nucleon–nucleon collisions at the same energy. This was experimentally observed in the most central heavy-ion collisions at SPS [8–10] and RHIC [11–13] energies.

At the significantly higher collision energies of the LHC, the suppression pattern of J/ψ mesons in heavy-ion collisions is fundamentally changed. In central Pb–Pb collisions at $\sqrt{s_{NN}} = 2.76$ TeV, where $\sqrt{s_{NN}}$ is the center-of-mass collision energy per nucleon–nucleon pair, the suppression was found to be weaker [14–16] in comparison with the earlier measurements at lower energies mentioned above. The effect was measured by the ALICE Collaboration at both mid- and forward rapidity, dominantly for J/ψ mesons at a low transverse momentum (p_T). This phenomenon is understood as the result of the charmonium (re)generation due to copiously produced charm quarks, made possible by the deconfined nature of the QGP. In addition to the weaker nuclear suppression of charmonia, recent observations of non-zero elliptic flow of D [17,18] and J/ψ [19] mesons, suggest that charm quarks may thermalize and flow with the bulk particles during the QGP phase.

There are different phenomenological scenarios available for the description of charmonium production in heavy-ion collisions. In the framework of statistical hadronization, all charmonium states are created at chemical equilibrium at the phase boundary and their abundances are determined by thermal weights [20,21]. The transport approach considers a continuous production and dissociation of charmonium states already during the QGP phase governed by a set of rate equations [22]. Another approach includes charmonium dissociation by the scattering of comoving partons and hadrons with a (re)generation component at LHC collision energies [23]. All current models implementing statistical hadronization, microscopic transport approaches [24,25] or comover interac-

* E-mail address: alice-publications@cern.ch.

tions take into account both the hot medium and the cold nuclear matter (CNM) [26] effects mainly originating from the modification of the gluon distribution function in the nucleus compared to the corresponding function of the free nucleon.

In this paper, we present the ALICE measurement of the inclusive J/ψ production at midrapidity in Pb–Pb collisions at a center-of-mass energy per nucleon pair of 5.02 TeV. The J/ψ mesons are reconstructed in the central barrel within the rapidity range $|y| < 0.9$ via the e^+e^- decay channel down to $p_T = 0$ GeV/c. The J/ψ p_T spectrum is measured in three centrality intervals. The J/ψ average transverse momentum $\langle p_T \rangle$ and $\langle p_T^2 \rangle$ are evaluated as a function of collision centrality: the latter is shown in comparison with the J/ψ $\langle p_T^2 \rangle$ measured in pp collisions, via the ratio $r_{AA} = \langle p_T^2 \rangle_{\text{PbPb}} / \langle p_T^2 \rangle_{\text{pp}}$. The nuclear modification factor R_{AA} , which is defined by the ratio of the production yield in Pb–Pb collisions and the production cross section in pp collisions normalized by the nuclear overlap function $\langle T_{AA} \rangle$, as a function of event centrality and J/ψ p_T , is obtained using the recent ALICE measurement of the inclusive J/ψ cross section in pp collisions at $\sqrt{s} = 5.02$ TeV [27]. The new pp reference and the larger Pb–Pb data set allow for a significant reduction of the uncertainties compared to our previous measurements at $\sqrt{s_{NN}} = 2.76$ TeV [14,28]. The results are compared with statistical [20], microscopic parton transport [24,25], and comover [23] model calculations.

The measurements presented in this publication provide a significant complement to results in Pb–Pb collisions at the same collision energy by the ALICE Collaboration at forward rapidity [29], the measurements on J/ψ suppression at high p_T by the ATLAS [30] and CMS [31] Collaborations around midrapidity, as well as to results at forward rapidity in Xe–Xe collisions at $\sqrt{s_{NN}} = 5.44$ TeV [32].

2. Apparatus and data sample

A detailed description of the ALICE detector and its performance can be found in Refs. [33,34]. The ALICE central barrel detector allows for high resolution tracking and particle identification over the full azimuthal angle in the pseudorapidity range $|\eta| < 0.9$. The entire setup is placed inside a solenoidal magnet, which creates a uniform axial magnetic field of $B = 0.5$ T along the beam direction.

The main detectors used for the J/ψ meson reconstruction in the e^+e^- decay channel are the Inner Tracking System (ITS) [35] and the Time Projection Chamber (TPC) [36]. The ITS consists of 6 cylindrical layers of silicon detectors placed at radial distances to the beam line from 3.9 cm to 43 cm and provides high-precision tracking close to the interaction point as well as the determination of the primary vertex of the event. The two innermost layers form the Silicon Pixel Detector (SPD), the intermediate two layers are the Silicon Drift Detector (SDD), and the outermost layers are the Silicon Strip Detector (SSD).

Placed around the ITS, the TPC detector is a large cylindrical drift chamber extending radially from 85 cm to 250 cm from the nominal interaction point ($x = y = z = 0$ cm) and longitudinally between -250 cm and $+250$ cm. In addition to being the main tracking detector, the TPC also provides particle identification via the measurement of the specific energy loss (dE/dx) of charged particles in the detector gas.

The V0 detectors [37] consist of two scintillator arrays, VOA and VOC, which are located on both sides of the nominal interaction point at $z = 329$ cm and $z = -90$ cm and cover the pseudorapidity interval $2.8 \leq \eta \leq 5.1$ and $-3.7 \leq \eta \leq -1.7$. The centrality of the events, expressed in fractions of the total inelastic hadronic cross section, is determined via a Glauber fit to the V0 amplitude as described in [38–40]. In addition, the V0 detectors are used to provide a minimum-bias trigger (MB), defined as the coincidence of signals in both V0 arrays and the beam crossing.

The results presented in this paper are obtained using the MB trigger data collected during the 2015 LHC Pb–Pb run at a center-of-mass energy per nucleon pair of 5.02 TeV. Beam-gas events are rejected using timing selections on the signals from the V0 and Zero Degree Calorimeters [41]. Pileup events are rejected online based on V0, but also in the offline analysis based on the correlation between the V0 multiplicity and the number of tracks reconstructed in the TPC. All events must have a reconstructed primary vertex with a longitudinal position within ± 10 cm around the nominal interaction point. Only the events corresponding to the most central 90% of the Pb–Pb inelastic cross section (0–90%) are used in this analysis. For these events the MB trigger is fully efficient and the contamination by electromagnetic interactions is negligible. After all selections, a sample of 70 million events is available for analysis, corresponding to an integrated luminosity of $L_{\text{int}} \approx 10 \mu\text{b}^{-1}$.

3. Analysis methods

The J/ψ candidates are reconstructed using the e^+e^- decay channel. The selected electron candidates are tracks reconstructed using both the ITS and TPC detectors. They must have a minimum transverse momentum of 1 GeV/c and pseudorapidity in the range $|\eta| < 0.9$. Primary electrons are selected using a maximum distance-of-closest-approach to the event vertex of at most 1 cm and 3 cm in the transverse and longitudinal directions, respectively. Additionally, kink-daughters, i.e. secondary tracks from long-lived weak decays of charged particles, are removed from the analysis. In order to improve the resolution of track reconstruction and to reject secondary electrons from photon conversions in the detector material, the tracks are selected to have at least one hit in either of the two SPD layers. Electrons and positrons from photon conversions are further rejected using a prefilter method [27] in which track candidates forming pairs with an electron-positron invariant mass lower than 50 MeV/ c^2 are removed from any further pairing. In the TPC, the electron candidates are required to have at least 70 out of 159 possible space points attached to the track, which ensures good tracking and particle identification resolution.

Electrons are identified by requiring that the measured dE/dx in the TPC lies within a $\pm 3\sigma_e$ band around the expected value for electrons estimated from a parameterization of the Bethe formula, where σ_e is the particle identification (PID) resolution in the TPC for electrons. The hadron contamination is reduced by excluding tracks compatible with the proton or pion hypothesis within $\pm 3.5\sigma_{p,\pi}$.

The number of observed J/ψ is obtained by constructing the invariant mass distribution of all combinations of opposite-sign (OS) electron pairs from the same event. The top panels of Fig. 1 show the invariant mass distributions obtained in central (0–10%, left) and peripheral (60–90%, right) collisions together with the estimated background. The background is obtained using the distribution of OS pairs constructed by pairing electrons and positrons from different events, so-called mixed events (ME), which is scaled to match the same-event OS invariant mass distribution in two mass intervals on either side of the J/ψ signal region: $2.0 < m_{ee} < 2.5$ GeV/ c^2 and $3.2 < m_{ee} < 3.7$ GeV/ c^2 , where the J/ψ contribution is expected to be negligible. The raw J/ψ signal is then obtained by integrating the background-subtracted distribution in the mass window 2.92–3.16 GeV/ c^2 . The lower panels of Fig. 1 show the OS invariant mass distribution after background subtraction. Good agreement with the J/ψ invariant mass distribution from Monte Carlo (MC) simulation, normalized to the integral of the raw signal, is observed. The potentially remaining correlated background from semi-leptonic decays of $c\bar{c}$ and $b\bar{b}$ pairs is included in the systematic uncertainty.

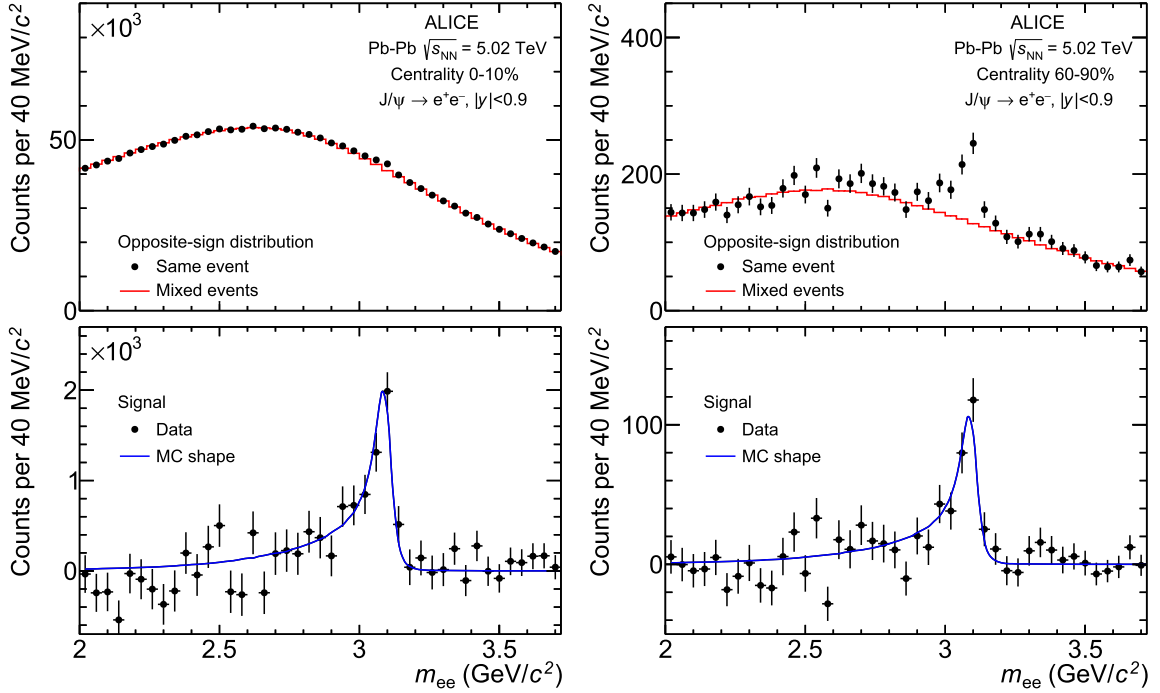


Fig. 1. Top panels: Invariant mass distribution of opposite-sign pairs from the same event and mixed events for the 0–10% (left) and 60–90% (right) centrality classes in Pb–Pb collisions at $\sqrt{s_{NN}} = 5.02$ TeV. Bottom panels: Background-subtracted invariant mass distributions in comparison with the expected Monte Carlo signal shape.

The corrected J/ψ p_T -differential production yield is obtained in a given centrality class as

$$\frac{d^2N}{dydp_T} = \frac{N_{J/\psi}}{N_{ev} \times BR_{J/\psi \rightarrow ee} \times (A \times \epsilon) \times \Delta y \times \Delta p_T}, \quad (1)$$

where $N_{J/\psi}$ is the number of reconstructed J/ψ in the considered centrality class and p_T and y intervals, N_{ev} is the corresponding number of events, $A \times \epsilon$ is the acceptance and efficiency correction factor and $BR_{J/\psi \rightarrow ee} = (5.971 \pm 0.032)\%$ is the branching ratio of the J/ψ decaying into the dielectron channel [42].

MC simulations of Pb–Pb collisions with embedded unpolarized J/ψ mesons are used to obtain the $A \times \epsilon$ factors. The Pb–Pb collisions are generated using HIJING [43]. For the J/ψ , the prompt component is generated using a p_T distribution tuned to the existing Pb–Pb measurements at forward rapidity while the non-prompt component is obtained from $b\bar{b}$ pairs generated with PYTHIA forced to decay into channels with J/ψ in the final state. The J/ψ decays into the e^+e^- channel are handled using PHOTOS [44]. The transport of the simulated particles in the detector material is performed using a GEANT3 [45] model of the ALICE apparatus and the same algorithm as for the real data is used to reconstruct the simulated tracks. The acceptance times efficiency correction factors include the kinematic acceptance, the reconstruction and PID efficiencies, and the fraction of signal in the integrated invariant mass window. The acceptance correction factor amounts to 33% and the fraction of the signal in the mass counting window is approximately 65%. Reconstruction and PID efficiencies are centrality dependent and together amount to approximately 24% in the most central collisions growing monotonically to approximately 32% in the most peripheral collisions. The correction factors are also p_T dependent which, for large p_T intervals, induces a dependence on the Monte Carlo p_T distribution of the embedded J/ψ . This is taken as a source of systematic uncertainty and is discussed in the following section. The inclusive p_T -integrated J/ψ production is measured in 5 different centrality classes: 0–10%, 10–20%, 20–40%, 40–60% and 60–90% while the p_T -differential cross sections are obtained in larger centrality

classes to ensure sufficient statistical significance: 0–20%, 20–40% and 40–90%.

The average transverse momentum of J/ψ , $\langle p_T \rangle$, is extracted using a binned log-likelihood fit of the $\langle p_T^{ee} \rangle$ distribution of all electron pairs as a function of the invariant mass. Each pair contribution is weighted by the $(A \times \epsilon)^{-1}$ factor corresponding to its centrality and p_T . The OS $\langle p_T^{ee} \rangle$ distribution is fitted with the function:

$$\langle p_T^{ee} \rangle(m_{ee}) = \frac{N^{bkg}(m_{ee}) \times \langle p_T^{bkg} \rangle(m_{ee}) + N^{J/\psi}(m_{ee}) \times \langle p_T \rangle}{N^{bkg}(m_{ee}) + N^{J/\psi}(m_{ee})}, \quad (2)$$

where $N^{bkg}(m_{ee})$ and $N^{J/\psi}(m_{ee})$ are the mass-dependent distributions of background and signal pairs determined via the signal extraction procedure described above. The background mean transverse momentum, $\langle p_T^{bkg} \rangle$, depends on the invariant mass and its shape is obtained from the ME technique, while its overall normalization can vary in the fit. Fig. 2 illustrates the $\langle p_T \rangle$ extraction procedure for the most central and most peripheral centrality intervals using dielectron pairs in the transverse momentum interval $0.15 < p_T < 10$ GeV/c. A similar procedure is employed also for the second moment of the transverse momentum distribution $\langle p_T^2 \rangle$.

A low- p_T cut-off on the J/ψ candidates is applied due to the observation of a J/ψ excess for $p_T < 0.3$ GeV/c at forward rapidity in peripheral Pb–Pb collisions at $\sqrt{s_{NN}} = 2.76$ TeV [46], which is found to originate from coherent photo-production. Since this production mechanism is not normally included in hadro-production models, the low- p_T interval is excluded for enabling comparisons with theoretical calculations. At midrapidity, mainly due to a better momentum resolution, nearly all of the coherent yield is contained in the range of reconstructed $p_T < 0.15$ GeV/c, as shown by the ALICE measurements of J/ψ photo-production in ultra-peripheral collisions [47]. A small component of incoherently photo-produced J/ψ is still present in the range $p_T < 1$ GeV/c, but for the centrality intervals considered in this work it is negligible. Thus, in the following, unless otherwise specified, all the results refer to J/ψ with p_T larger than 0.15 GeV/c.

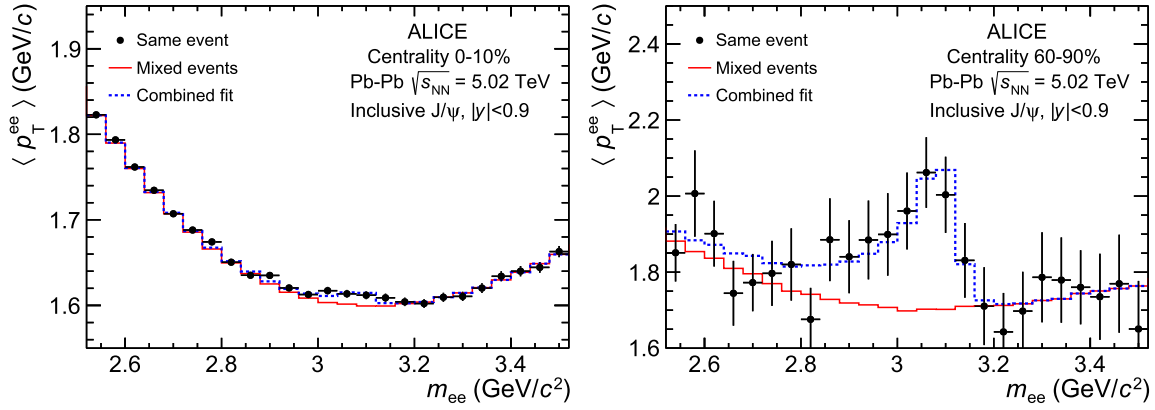


Fig. 2. Extraction of the J/ψ $\langle p_T \rangle$ in Pb-Pb collisions at $\sqrt{s_{NN}} = 5.02$ TeV for the 0–10% (left) and 60–90% (right) centrality classes in the transverse momentum interval $0.15 < p_T < 10$ GeV/c. The background, obtained from event-mixing, is shown by the red line.

Table 1

Average number of participant nucleons (N_{part}) and average nuclear overlap function ($\langle T_{AA} \rangle$) for the centrality classes used in this analysis. The values are derived from [40].

Centrality (%)	$\langle N_{part} \rangle$	$\langle T_{AA} \rangle$ (mb $^{-1}$)
0–10	357.3 ± 0.8	23.26 ± 0.17
0–20	309.7 ± 0.9	18.83 ± 0.14
10–20	262.0 ± 1.2	14.40 ± 0.13
20–40	159.4 ± 1.3	6.97 ± 0.09
40–60	70.7 ± 0.9	2.05 ± 0.04
40–90	39.0 ± 0.7	1.00 ± 0.03
60–90	17.9 ± 0.3	0.31 ± 0.01
0–90	125.9 ± 1.0	6.28 ± 0.12

The inclusive J/ψ nuclear modification factor is computed for a given centrality class as

$$R_{AA} = \frac{d^2N/dydp_T}{\langle T_{AA} \rangle d^2\sigma_{pp}/dydp_T}, \quad (3)$$

where $d^2N/dydp_T$ is the inclusive J/ψ yield defined in Equation 1, the $\langle T_{AA} \rangle$ is the average nuclear overlap function corresponding to the considered centrality class and $d^2\sigma_{pp}/dydp_T$ is the inclusive J/ψ cross section measured by ALICE in pp collisions at $\sqrt{s} = 5.02$ TeV [27]. The values used for the nuclear overlap function are shown in Table 1 and are obtained from [40].

4. Systematic uncertainties

The systematic uncertainties on the measured J/ψ yields, $\langle p_T \rangle$, and $\langle p_T^2 \rangle$ originate from uncertainties on tracking, electron identification, signal extraction procedure, the kinematics used in the MC simulation for estimating the $A \times \epsilon$ corrections, and the J/ψ decay branching ratio. For the R_{AA} and the r_{AA} , the uncertainties on the J/ψ cross section measurement in pp collisions [27] and (only in the case of the R_{AA}) on the nuclear overlap function ($\langle T_{AA} \rangle$) [40] need to be considered in addition. A summary of the uncertainties on the p_T -integrated and p_T -differential yields is given in Table 2.

The systematic uncertainty on the tracking of the candidate electrons is mainly due to uncertainties on the ITS-TPC track matching and on the track reconstruction efficiency in both the ITS and the TPC. These uncertainties, mainly due to differences in the reconstruction efficiency between data and MC, are estimated by varying the main track selection criteria and repeating the whole analysis chain. All variations which provide a corrected yield that deviates from the yield obtained with the standard selection criteria by more than one standard deviation are considered [48]. The tracking uncertainty is then obtained as the root-mean-square

Table 2

Systematic uncertainties on the p_T -integrated and on p_T -differential J/ψ yields for different centrality intervals. Only the ranges of uncertainty are quoted over the considered centrality intervals. The individual contributions and the total uncertainties are given as percent values.

Source	p_T -integrated	p_T -differential	$\langle p_T \rangle$	r_{AA}
Tracking	2–7	4–9	2–4	3–6
PID	3–6	1–6	1–2	2–4
Signal extraction	2–7	5–7	1–2	2–3
MC input	2	1–2	n.a.	n.a.
$\langle T_{AA} \rangle$	2–5	2–5	n.a.	n.a.
pp reference	7	9–12	3	5

of the distribution of all the valid variations, while the distribution mean is used as the central value. For the J/ψ yields, this uncertainty ranges between 2% and 7% as a function of centrality (integrated over p_T) and between 4% and 9% as a function of transverse momentum. The tracking systematic uncertainty on the $\langle p_T \rangle$ and $\langle p_T^2 \rangle$ are smaller than those for the corrected yields and detailed in Table 2.

Uncertainties on the electron identification are due to the TPC electron PID response and the hadron rejection. A data-driven procedure is used to improve the matching between data and simulation for the electron selection by employing a pure sample of electrons from tagged photon conversions in the detector material. The residual mismatches are estimated by varying all the PID selection criteria following a similar procedure as for the tracking systematic uncertainty. The extracted uncertainty on the J/ψ yields ranges between 1% and 6%, depending on the centrality and transverse momentum interval.

The uncertainty from the signal extraction procedure includes two components, one due to the J/ψ signal shape and one due to the residual correlated dielectron background in the J/ψ mass region. In order to estimate the uncertainty on the signal shape, the corrected J/ψ yields are estimated using variations of the standard signal counting mass region, 2.92–3.16 GeV/ c^2 . For this we used three additional values of the lower mass limit, between 2.92 and 2.80 GeV/ c^2 and two additional values for the upper mass limit, namely 3.12 and 3.20 GeV/ c^2 . The correlated dielectron background in the invariant mass range used to extract the signal has generally a different shape compared to the combinatorial background. So matching the ME background in the sidebands of the same-event OS distribution may lead to a bias in the estimation of the raw yields. This is taken as a systematic uncertainty and is estimated by varying the mass ranges of the sidebands where the ME background is matched. By these variations the width of the sidebands was modified between 400 and 800 MeV/ c^2 . The total uncertainty on the signal extraction ranges between 2% to 7%

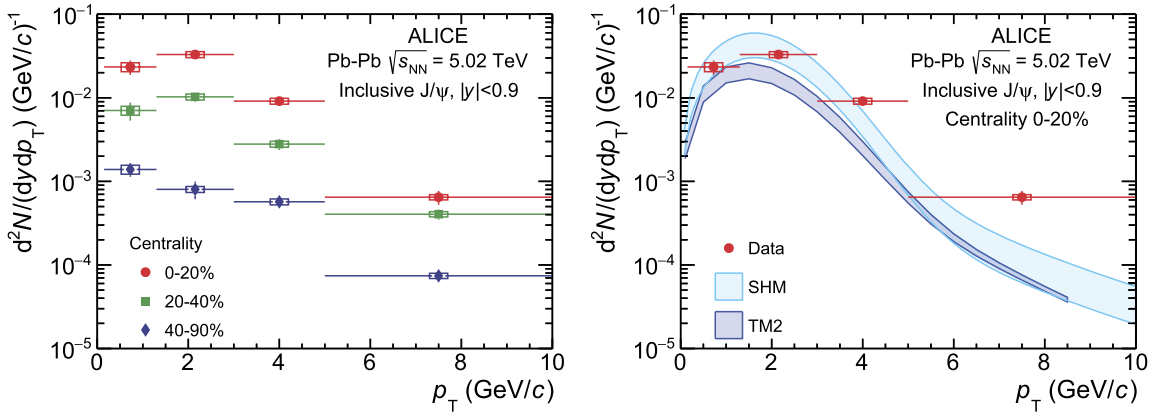


Fig. 3. Left panel: Transverse momentum dependence of the J/ψ production yields in Pb-Pb collisions at $\sqrt{s_{NN}} = 5.02$ TeV at midrapidity in the centrality intervals 0–20%, 20–40%, and 40–90%. Right panel: Comparison of the p_T distribution in the centrality interval 0–20% with models [25,49].

as a function of centrality and between 5% and 7% as a function of p_T .

The acceptance and efficiency correction is p_T dependent which makes correction factors averaged over large p_T intervals sensitive to the J/ψ p_T spectrum used in the simulation. Since precise measurements of the J/ψ transverse momentum spectra at midrapidity down to $p_T = 0$ GeV/c are not available, the simulations used for corrections rely on the ALICE measurement at forward rapidity ($2.5 < y < 4.0$) in Pb-Pb collisions at $\sqrt{s_{NN}} = 5.02$ TeV [29]. The measured spectrum including the statistical and systematic uncertainties is fitted using a power law function and the fit parameters are varied randomly within their allowed uncertainties taking into account their correlation matrix. The resulting uncertainty amounts to 2% for the p_T -integrated corrected yields and ranges between 1% to 2% in the considered p_T intervals.

Systematic uncertainties on the extraction of $\langle p_T \rangle$ and $\langle p_T^2 \rangle$ are obtained by repeating the fit procedure with similar variations of tracking and PID selections as for the yield estimation. Since for this measurement the $A \times \epsilon$ correction is applied for each dielectron pair using a fine-binned distribution of the correction factors, the systematic uncertainty due to the kinematics of the J/ψ used in the MC simulation is negligible. In addition, the $\langle p_T \rangle$ and $\langle p_T^2 \rangle$ are also extracted by directly fitting the corrected J/ψ spectrum with a power law function and are found to be compatible to the values obtained from the fit with Equation 2.

Systematic uncertainties on the tracking, PID and MC kinematics are considered to be partly correlated over both the centrality and the transverse momentum. The systematic uncertainties on signal extraction are considered as uncorrelated. The uncertainties on the nuclear overlap function are taken as uncorrelated over centrality and fully correlated over p_T within a given centrality interval. The uncertainty on the p_T -integrated pp reference is considered to be fully correlated over centrality, while the uncertainties on the p_T -differential values are fully correlated over centrality and highly correlated over p_T .

5. Results and discussions

The inclusive J/ψ p_T -differential yields evaluated using Equation 1 are shown in the left panel of Fig. 3 (left) for the 0–20%, 20–40%, and 40–90% centrality intervals. The vertical error bars indicate statistical uncertainties while the systematic uncertainties, independently of their degree of correlation, are shown as boxes around the data points. The horizontal error bars show the evaluated p_T -range with the data point placed in the center.

The experimental results are compared with different phenomenological models of the charmonium production in relativistic heavy-ion collisions, i.e. the statistical hadronization model

(SHM) by Andronic et al. [21], the comover interaction model (CIM) by Ferreira [23,50] and two different microscopic transport models, by Zhao et al. (TM1) [24] and by Zhou et al. (TM2) [25].

In the SHM, all heavy quarks are produced during the initial hard partonic interactions followed by their thermalization in the QGP and the subsequent formation of bound states at the phase boundary according to their thermal weights. The p_T -integrated charmed-hadron yields depend only on the total $c\bar{c}$ cross section in heavy-ion collisions and on the chemical freeze-out parameters, which are determined by fitting measured light-flavored hadron yields. In addition to the high-density core part in the QGP, a corona contribution is added for the case that the nuclear density decreases below 10% of its maximal value, where no QGP is assumed and the number of J/ψ is calculated from yields in pp collisions scaled by the number of binary nucleon-nucleon collision. A recent update of the SHM [49] uses a MUSIC (3+1)D [51] hydrodynamical simulation to extract the transverse flow velocity and the radial velocity profile of the freeze-out hyper-surface, such that the J/ψ p_T can be extracted from a blast-wave parameterization which follows a Hubble-like expansion [52].

The CIM [23] was developed specifically for the description of charmonium suppression in heavy-ion collisions via its interactions with a comoving medium, either hadronic or partonic. The hot medium effects are modeled using a rate equation which contains a loss term for charmonium dissociation, and a gain term for (re)generation. In this model, the charmonium dissociation rate depends on the density of comovers, obtained from experimental measurements and on the charmonium dissociation cross section which is an energy-independent parameter of the model, fixed from fits to low energy data. Charmonium dissociation is balanced by the (re)generation component which depends on the primordial charm-quark cross section.

Both microscopic transport models considered here, TM1 [24] and TM2 [25], solve the Boltzmann equation for charmonia (J/ψ , χ_c and ψ') with dissociation and recombination terms. Each model considers the fireball evolution using implementations of ideal hydrodynamics which include both the deconfined and the hadronic phase separated by a first order phase transition. The dissociation rate in both models depends on the medium density and on a lattice-QCD-inspired charmonium binding energy (in TM1) or squared radius of the bound state (in TM2), all of them being functions of temperature. The (re)generation component is implemented using different approaches. In the TM1 calculations, it is based on the assumption that the charm quarks reach statistical equilibration after a relaxation time of about a few fm/c, while in the TM2 calculations the charm quarks are recombined using the

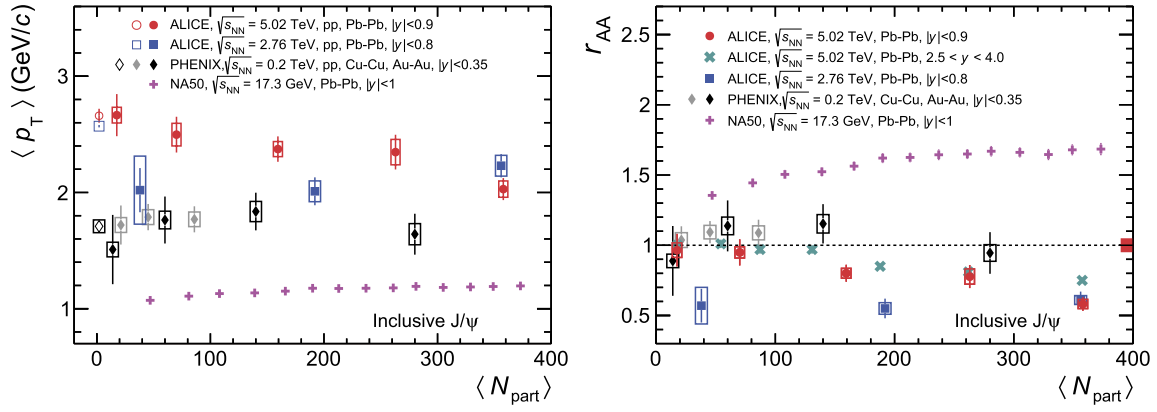


Fig. 4. J/ψ (p_T) (left) and r_{AA} (right) at midrapidity as a function of the mean number of participant nucleons ($\langle N_{part} \rangle$). The ALICE measurements at $\sqrt{s_{NN}} = 5.02$ TeV are compared with previous results in pp and Pb–Pb collisions at 2.76 TeV [28], Pb–Pb collisions at 5.02 at forward rapidity [53], and with those at lower collision energies at SPS [54] and RHIC [11,55,56]. The red box around unity at $N_{part} \approx 400$ in the right panel indicates the correlated uncertainty of the ALICE data points due to the $\langle p_T^2 \rangle$ in pp collisions.

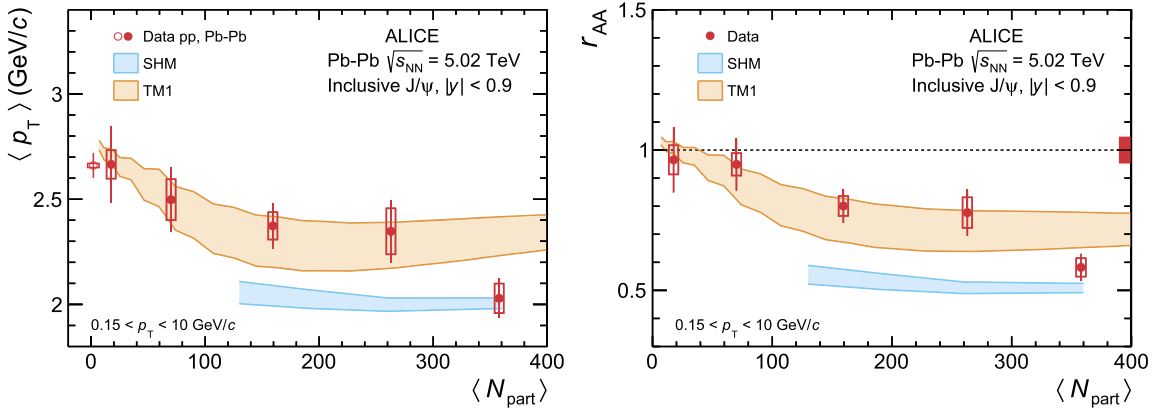


Fig. 5. Inclusive J/ψ (p_T) (left) and r_{AA} (right) in pp [27] and Pb–Pb collisions at $\sqrt{s_{NN}} = 5.02$ TeV at midrapidity as a function of the mean number of participating nucleons. The ALICE results are compared with calculations from the transport models [57,58] and the SHM [49]. The colored bands represent model uncertainties. As in Fig. 4, the red box around unity at $N_{part} \approx 400$ in the right panel indicates the correlated uncertainty of the ALICE data points due to the $\langle p_T^2 \rangle$ in pp collisions.

same cross section as for the dissociation process and a thermalized distribution of charm quarks.

The primordial $c\bar{c}$ production cross section in Pb–Pb collisions is a common input for all of the above mentioned models. There is so far no measurement of the $c\bar{c}$ cross section in Pb–Pb or pp collisions at $\sqrt{s_{NN}} = 5.02$ TeV at midrapidity, which lead dominantly to the uncertainty of the models. The cross section in Pb–Pb collisions is obtained from the total $c\bar{c}$ cross section in pp collisions $d\sigma_{c\bar{c}}/dy$ scaled by the average number of nucleon–nucleon collisions $\langle N_{coll} \rangle$ in a given centrality class of Pb–Pb collisions with additional CNM effects taken into account. For the rapidity interval used in this work, $|y| < 0.9$, the value of $d\sigma_{c\bar{c}}/dy$ estimated for MB Pb–Pb collisions is 0.53 ± 0.10 mb for the SHM, 0.76 ± 0.13 mb for TM1, 0.78 ± 0.09 mb for TM2 and 0.56 ± 0.11 mb for CIM.

The right panel of Fig. 3 shows a comparison of the inclusive J/ψ transverse momentum spectrum in the 20% most central Pb–Pb collisions to calculations from the SHM and TM2 models. The bands indicate model uncertainties mainly due to the assumptions on the $d\sigma_{c\bar{c}}/dy$. Good agreement between data and the SHM predictions is observed in the low- p_T region, while for $p_T \gtrsim 5$ GeV/c the calculations underestimate the data. The TM2 calculations underestimate the measured yields over the measured p_T range.

In order to facilitate the comparison of the J/ψ p_T spectra obtained in this work with other measurements or theory calculations, the J/ψ (p_T) and $\langle p_T^2 \rangle$ are extracted in several centrality intervals, using the method described in Sec. 3. The left panel

of Fig. 4 shows the J/ψ (p_T) dependence on the mean number of participant nucleons ($\langle N_{part} \rangle$). The $\langle p_T \rangle$ in Pb–Pb collisions at $\sqrt{s_{NN}} = 5.02$ TeV shows a monotonic decrease from the most peripheral collisions, where it is compatible to the measurement in pp collisions at $\sqrt{s} = 5.02$ TeV, to the most central collisions, which hints towards a strong contribution from (re)combination processes. This trend is not clearly visible for the measurement at $\sqrt{s_{NN}} = 2.76$ TeV, which suffered from large statistical and systematic uncertainties.

The r_{AA} ratio, defined as $\langle p_T^2 \rangle_{PbPb} / \langle p_T^2 \rangle_{pp}$, which is shown in the right panel of Fig. 4, is a measure of the broadness of the p_T spectra in heavy-ion collisions relative to pp collisions at the same energy. A strong decrease of the r_{AA} is observed in Pb–Pb collisions at $\sqrt{s_{NN}} = 5.02$ TeV between peripheral, where it is consistent with unity, and central collisions where r_{AA} reaches a value of 0.6 at midrapidity and 0.75 at forward rapidity [53]. When comparing with measurements at lower energies from RHIC [11,55,56] and SPS [54], a very different picture emerges. While the RHIC measurements for both $\langle p_T \rangle$ and r_{AA} are compatible with a constant trend as a function of $\langle N_{part} \rangle$ [25], the SPS results show a monotonic increase of both $\langle p_T \rangle$ and r_{AA} as a function of collision centrality which, at this energy, can be explained by a broadening of the p_T distribution due to the Cronin effect [59].

The results for the $\langle p_T \rangle$ and r_{AA} in Pb–Pb collisions at $\sqrt{s_{NN}} = 5.02$ TeV are compared with model calculations in Fig. 5. The statistical hadronization model agrees with the data only for the most central collisions but underestimates the measurements for more

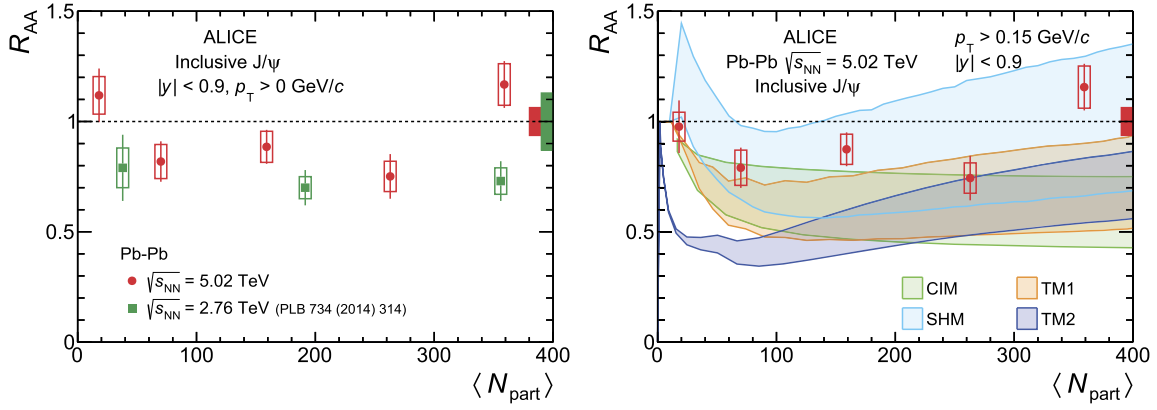


Fig. 6. Inclusive J/ψ nuclear modification factor at midrapidity, integrated over p_T , as a function of $\langle N_{\text{part}} \rangle$ in Pb–Pb collisions at $\sqrt{s_{\text{NN}}} = 5.02$ TeV compared with results at $\sqrt{s_{\text{NN}}} = 2.76$ TeV [14] (left panel) and with calculations from the CIM [23], SHM [49], TM1 [58] and TM2 [25] models (right panel). The yields in the left panel are shown without the low- p_T cut-off in order to be able to compare with the lower energy data which are obtained for $p_T > 0$. The calculations are shown as bands indicating the model uncertainties. Boxes around unity at $N_{\text{part}} \approx 400$ in both panels indicate the correlated uncertainty of the data points due to the cross section in pp collisions.

peripheral collisions. A good description of the centrality trend is obtained with the transport model TM1 calculation, which includes a detailed implementation of the fireball evolution, with the exception of most central collisions where the model overestimates both the J/ψ $\langle p_T \rangle$ and r_{AA} .

The p_T -integrated nuclear modification factor for inclusive J/ψ in Pb–Pb collisions at $\sqrt{s_{\text{NN}}} = 5.02$ TeV obtained using Equation 3 is shown in the left panel of Fig. 6 as a function of the mean number of participants and compared with a measurement at $\sqrt{s_{\text{NN}}} = 2.76$ TeV [14]. The boxes shown around unity indicate the correlated systematic uncertainties and include the uncertainties on the pp reference. Besides the most central collisions where there is a hint of an increase of the R_{AA} with collision energy, the results at the two energies are compatible within uncertainties. A comparison of the experimental results at $\sqrt{s_{\text{NN}}} = 5.02$ TeV with calculations based on the models described before is shown in the right panel of Fig. 6. The calculations are shown as bands that indicate model uncertainties, dominated by the uncertainties on the $c\bar{c}$ cross section and on the CNM effects. The SHM calculation shows a good agreement with the data over the entire centrality range. CIM, TM1 and TM2 calculations underestimate the experimental results towards the data points corresponding to the most central collisions despite the fact that the total $c\bar{c}$ cross section assumed in TM1 and TM2 is significantly larger compared to the SHM and the CIM. The large model uncertainties do not allow a conclusion to be made on the phenomenology of charmonium production in nuclear collisions. This emphasizes the importance of a precise measurement of the total $c\bar{c}$ cross section, but also the need of using consistent model inputs, including the total $c\bar{c}$ cross section, the pp reference J/ψ cross section and CNM effects.

The inclusive J/ψ nuclear modification factor in Pb–Pb collisions as a function of p_T is shown in the left panel of Fig. 7 for the centrality intervals 0–20%, 20–40% and 40–90%. The systematic uncertainties shown as boxes around the data points include the systematic uncertainties from the Pb–Pb analysis while the uncertainties from the pp reference, correlated over centrality, are shown as the gray band around unity. The colored boxes at high p_T around unity indicate the correlated uncertainties due to the $\langle T_{AA} \rangle$ values used for the R_{AA} calculation. These results are compatible with binary scaling for $p_T < 3$ GeV/c, with the exception of the data point around 2 GeV/c which shows a downward statistical fluctuation for 40–90% centrality, while the J/ψ production is suppressed at higher p_T . With the current uncertainties it is difficult to extract a centrality trend except for the highest p_T interval, 5–10 GeV/c, where a stronger suppression is observed in the most central collisions relative to the more peripheral centrality inter-

vals at a significance level of about 3σ . The results for the 20% most central collisions are compared with model calculations and shown in the right panel of Fig. 7. Both the SHM and TM1 models describe qualitatively the data. In these models, the increasing R_{AA} towards low p_T is a consequence of the dominant contribution of (re)generated J/ψ . At high p_T , the contribution from recombination decreases, and the J/ψ production is suppressed due to color charges in the medium. The main J/ψ sources at high p_T are primordial production and feed-down from beauty decays. The SHM, where the J/ψ at high p_T are produced only in the corona, overestimates the degree of J/ψ suppression.

Since the charm quark density, i.e. the $c\bar{c}$ cross section, is expected to decrease towards larger rapidity, the comparison to the forward-rapidity measurements is a valuable source of information. In the left panel of Fig. 8, the p_T dependence of the J/ψ R_{AA} in the 20% most central Pb–Pb collisions at midrapidity is compared with the ALICE results measured at forward rapidity ($2.5 < y < 4$) [29]. The boxes around the data points represent systematic uncertainties, while the boxes drawn around $R_{AA} = 1$ show global uncertainties on the pp reference due to uncertainties on the beam luminosity and $\langle T_{AA} \rangle$. In the low- p_T range ($p_T < 5$ GeV/c) these data indicate larger R_{AA} values at midrapidity compared to those at forward rapidity, with a combined statistical significance of nearly 4σ , compatible with expectations from a (re)generation scenario due to the larger primordial $c\bar{c}$ density at midrapidity. The rapidity dependence of the inclusive J/ψ suppression, integrated over p_T , is shown in the right panel of Fig. 8 for the 0–90% centrality interval. The value of the R_{AA} at midrapidity is $0.97 \pm 0.05(\text{stat.}) \pm 0.1(\text{syst.})$, and a monothonic decrease is observed towards forward rapidity [29,53].

6. Conclusions

The measurements of the inclusive J/ψ yields and nuclear modification factors at midrapidity ($|y| < 0.9$) were performed in the dielectron decay channel in Pb–Pb collisions at a center-of-mass energy $\sqrt{s_{\text{NN}}} = 5.02$ TeV using an integrated luminosity of $L_{\text{int}} \approx 10 \mu\text{b}^{-1}$ collected by the ALICE Collaboration. The results were presented as a function of transverse momentum in different collision centrality classes.

The J/ψ transverse momentum dependent yields in central Pb–Pb collisions are well reproduced in the low p_T range by an updated SHM calculation [49] and underestimated for large p_T . The TM2 [25] transport calculations underestimate the J/ψ yields over the entire measured p_T range. The J/ψ $\langle p_T \rangle$ and $\langle p_T^2 \rangle$ show a decrease from peripheral collisions, where they are similar to the

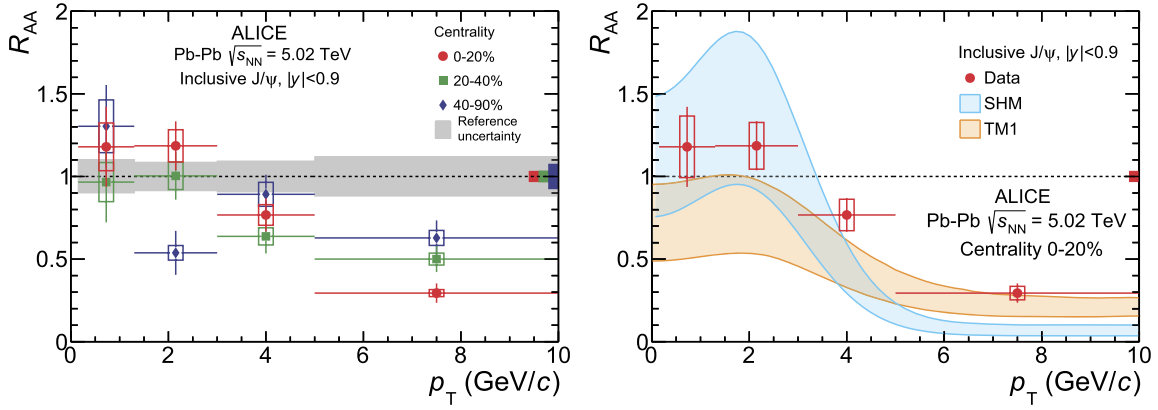


Fig. 7. Inclusive J/ψ R_{AA} at midrapidity in Pb-Pb collisions at $\sqrt{s_{NN}} = 5.02$ TeV as a function of p_T for different centrality intervals (left) and compared with model calculations [49,58] for the centrality interval 0–20% (right).

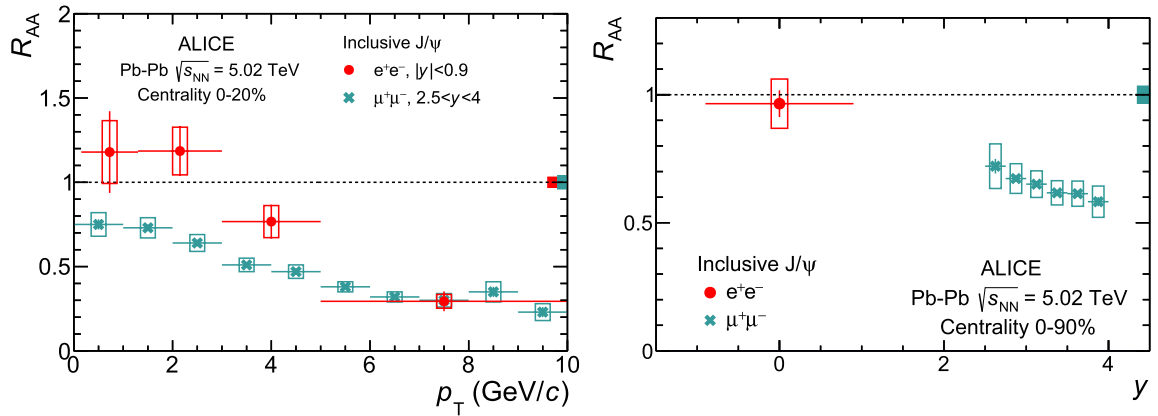


Fig. 8. Left: Inclusive J/ψ R_{AA} in the 20% most central Pb-Pb collisions at $\sqrt{s_{NN}} = 5.02$ TeV as a function of p_T , at midrapidity and at forward rapidity [29,53]. Right: Rapidity dependence of the inclusive J/ψ R_{AA} in the centrality interval 0–90%. The error bars represent statistical uncertainties, while the boxes around the data points represent systematic uncertainties. The boxes around unity represent global uncertainties on the pp reference due to normalization and $\langle T_{AA} \rangle$. In the right panel, the correlated uncertainty of the point at midrapidity is included in the box around the data point.

values observed in pp collisions, towards most central collisions. This centrality-dependent behavior is qualitatively different compared to the observations at lower energies from RHIC and SPS and can be explained through the interplay between the (re)generation process, dominant at low p_T for central events at the LHC, color screening, and CNM effects like gluon shadowing. A good description of the observed trends is provided by the TM1 calculations, while the SHM calculations agree with the data for central collisions only.

The p_T -integrated nuclear modification factor as a function of the number of participant nucleons shows a moderate level of suppression in the range $50 < \langle N_{part} \rangle < 300$, and indicates an increase towards central collisions. In the most peripheral collisions, our results are compatible with binary scaling of the J/ψ production. The nuclear modification factor as a function of the transverse momentum shows a strong suppression, centrality dependent, for $p_T > 3$ GeV/c but is compatible with unity or with a small enhancement at small p_T , suggestive of the large contribution from the (re)generation process. Furthermore, from these measurements we observe significantly larger values for R_{AA} compared to the results at forward rapidity [29] for both the p_T -integrated values in the 0–90% centrality interval and for the p_T -differential R_{AA} in the low p_T region ($p_T < 5$ GeV/c) in the centrality interval 0–20%.

Consequently, these results strengthen the hypothesis that charmonium at low p_T is produced predominantly via (re)generation in the late stages of the collision at the LHC. However, due to the remaining experimental and theoretical uncertainties, the exact phe-

nomenology leading to these observations cannot be determined yet.

Declaration of competing interest

The authors declare that they have no known competing financial interests or personal relationships that could have appeared to influence the work reported in this paper.

Acknowledgements

The ALICE Collaboration would like to thank all its engineers and technicians for their invaluable contributions to the construction of the experiment and the CERN accelerator teams for the outstanding performance of the LHC complex. The ALICE Collaboration gratefully acknowledges the resources and support provided by all Grid centres and the Worldwide LHC Computing Grid (WLCG) collaboration. The ALICE Collaboration acknowledges the following funding agencies for their support in building and running the ALICE detector: A. I. Alikhanyan National Science Laboratory (Yerevan Physics Institute) Foundation (ANSL), State Committee of Science and World Federation of Scientists (WFS), Armenia; Austrian Academy of Sciences, Austrian Science Fund (FWF): [M 2467-N36] and Nationalstiftung für Forschung, Technologie und Entwicklung, Austria; Ministry of Communications and High Technologies, National Nuclear Research Center, Azerbaijan; Conselho Nacional de Desenvolvimento Científico e Tecnológico (CNPq), Financiadora de Estudos e Projetos (Finep), Fundação de Amparo à

Pesquisa do Estado de São Paulo (FAPESP) and Universidade Federal do Rio Grande do Sul (UFRGS), Brazil; Ministry of Education of China (MOEC), Ministry of Science & Technology of China (MSTC) and National Natural Science Foundation of China (NSFC), China; Ministry of Science and Education and Croatian Science Foundation, Croatia; Centro de Aplicaciones Tecnológicas y Desarrollo Nuclear (CEADEN), Cubaenergía, Cuba; Ministry of Education, Youth and Sports of the Czech Republic, Czech Republic; The Danish Council for Independent Research | Natural Sciences, the Villum Fonden and Danish National Research Foundation (DNRF), Denmark; Helsinki Institute of Physics (HIP), Finland; Commissariat à l'Énergie Atomique (CEA), Institut National de Physique Nucléaire et de Physique des Particules (IN2P3) and Centre National de la Recherche Scientifique (CNRS) and Région des Pays de la Loire, France; Bundesministerium für Bildung und Forschung (BMBF) and GSI Helmholtzzentrum für Schwerionenforschung GmbH, Germany; General Secretariat for Research and Technology, Ministry of Education, Research and Religions, Greece; National Research Development and Innovation Office, Hungary; Department of Atomic Energy, Government of India (DAE), Department of Science and Technology, Government of India (DST), University Grants Commission, Government of India (UGC) and Council of Scientific and Industrial Research (CSIR), India; Indonesian Institute of Science, Indonesia; Centro Fermi - Museo Storico della Fisica e Centro Studi e Ricerche Enrico Fermi and Istituto Nazionale di Fisica Nucleare (INFN), Italy; Institute for Innovative Science and Technology, Nagasaki Institute of Applied Science (IIST), Japanese Ministry of Education, Culture, Sports, Science and Technology (MEXT) and Japan Society for the Promotion of Science (JSPS) KAKENHI, Japan; Consejo Nacional de Ciencia (CONACYT) y Tecnología, through Fondo de Cooperación Internacional en Ciencia y Tecnología (FONCICYT) and Dirección General de Asuntos del Personal Académico (DGAPA), Mexico; Nederlandse Organisatie voor Wetenschappelijk Onderzoek (NWO), Netherlands; The Research Council of Norway, Norway; Commission on Science and Technology for Sustainable Development in the South (COMSATS), Pakistan; Pontificia Universidad Católica del Perú, Peru; Ministry of Science and Higher Education and National Science Centre, Poland; Korea Institute of Science and Technology Information and National Research Foundation of Korea (NRF), Republic of Korea; Ministry of Education and Scientific Research, Institute of Atomic Physics and Ministry of Research and Innovation and Institute of Atomic Physics, Romania; Joint Institute for Nuclear Research (JINR), Ministry of Education and Science of the Russian Federation, National Research Centre Kurchatov Institute, Russian Science Foundation and Russian Foundation for Basic Research, Russia; Ministry of Education, Science, Research and Sport of the Slovak Republic, Slovakia; National Research Foundation of South Africa, South Africa; Swedish Research Council (VR) and Knut & Alice Wallenberg Foundation (KAW), Sweden; European Organization for Nuclear Research, Switzerland; Suranaree University of Technology (SUT), National Science and Technology Development Agency (NSDTA) and Office of the Higher Education Commission under NRU project of Thailand, Thailand; Turkish Atomic Energy Agency (TAEK), Turkey; National Academy of Sciences of Ukraine, Ukraine; Science and Technology Facilities Council (STFC), United Kingdom; National Science Foundation of the United States of America (NSF) and United States Department of Energy, Office of Nuclear Physics (DOE NP), United States of America.

References

- [1] A. Bazavov, et al., Equation of state and QCD transition at finite temperature, *Phys. Rev. D* 80 (2009) 014504.
- [2] S. Borsanyi, Z. Fodor, C. Hoelbling, S.D. Katz, S. Krieg, K.K. Szabo, Full result for the QCD equation of state with 2+1 flavors, *Phys. Lett. B* 730 (2014) 99–104, arXiv:1309.5258 [hep-lat].
- [3] ALICE Collaboration, S. Acharya, et al., Kaon femtoscopy in Pb-Pb collisions at $\sqrt{s_{NN}} = 2.76$ TeV, *Phys. Rev. C* 96 (6) (2017) 064613, arXiv:1709.01731 [nucl-ex].
- [4] A. Andronic, et al., Heavy-flavour and quarkonium production in the LHC era: from proton-proton to heavy-ion collisions, *Eur. Phys. J. C* 76 (3) (2016) 107, arXiv:1506.03981 [nucl-ex].
- [5] A. Mocsy, P. Petreczky, M. Strickland, Quarkonia in the quark gluon plasma, *Int. J. Mod. Phys. A* 28 (2013) 1340012, arXiv:1302.2180 [hep-ph].
- [6] T. Matsui, H. Satz, J/ψ suppression by quark-gluon plasma formation, *Phys. Lett. B* 178 (1986) 416–422.
- [7] F. Karsch, D. Kharzeev, H. Satz, Sequential charmonium dissociation, *Phys. Lett. B* 637 (2006) 75–80, arXiv:hep-ph/0512239 [hep-ph].
- [8] NA38 Collaboration, C. Baglin, et al., $\psi(2S)$ and J/ψ production in p-W, p-U and S-U interactions at 200-GeV/nucleon, *Phys. Lett. B* 345 (1995) 617–621.
- [9] NA50 Collaboration, B. Alessandro, et al., A new measurement of J/ψ suppression in Pb-Pb collisions at 158-GeV per nucleon, *Eur. Phys. J. C* 39 (2005) 335–345, arXiv:hep-ex/0412036 [hep-ex].
- [10] NA60 Collaboration, R. Arnaldi, et al., J/ψ production in indium-indium collisions at 158 GeV/nucleon, *Phys. Rev. Lett.* 99 (2007) 132302.
- [11] PHENIX Collaboration, A. Adare, et al., J/ψ production vs centrality, transverse momentum, and rapidity in Au-Au collisions at $\sqrt{s_{NN}} = 200$ GeV, *Phys. Rev. Lett.* 98 (2007) 232301, arXiv:nucl-ex/0611020 [nucl-ex].
- [12] PHENIX Collaboration, A. Adare, et al., J/ψ suppression at forward rapidity in Au-Au collisions at $\sqrt{s_{NN}} = 200$ GeV, *Phys. Rev. C* 84 (2011) 054912, arXiv:1103.6269 [nucl-ex].
- [13] STAR Collaboration, L. Adamczyk, et al., J/ψ production at low p_T in Au-Au and Cu-Cu collisions at $\sqrt{s_{NN}} = 200$ GeV with the STAR detector, *Phys. Rev. C* 90 (2) (2014) 024906, arXiv:1310.3563 [nucl-ex].
- [14] ALICE Collaboration, B. Abelev, et al., Centrality, rapidity and transverse momentum dependence of J/ψ suppression in Pb-Pb collisions at $\sqrt{s_{NN}} = 2.76$ TeV, *Phys. Lett. B* 734 (2014) 314–327, arXiv:1311.0214 [nucl-ex].
- [15] ALICE Collaboration, B. Abelev, et al., J/ψ suppression at forward rapidity in Pb-Pb collisions at $\sqrt{s_{NN}} = 2.76$ TeV, *Phys. Rev. Lett.* 109 (2012) 072301, arXiv:1202.1383 [hep-ex].
- [16] ALICE Collaboration, J. Adam, et al., Differential studies of inclusive J/ψ and $\psi(2S)$ production at forward rapidity in Pb-Pb collisions at $\sqrt{s_{NN}} = 2.76$ TeV, *J. High Energy Phys.* 05 (2016) 179, arXiv:1506.08804 [nucl-ex].
- [17] CMS Collaboration, A.M. Sirunyan, et al., Measurement of prompt D^0 meson azimuthal anisotropy in Pb-Pb collisions at $\sqrt{s_{NN}} = 5.02$ TeV, *Phys. Rev. Lett.* 120 (20) (2018) 202301, arXiv:1708.03497 [nucl-ex].
- [18] ALICE Collaboration, S. Acharya, et al., D -meson azimuthal anisotropy in mid-central Pb-Pb collisions at $\sqrt{s_{NN}} = 5.02$ TeV, *Phys. Rev. Lett.* 120 (10) (2018) 102301, arXiv:1707.01005 [nucl-ex].
- [19] ALICE Collaboration, S. Acharya, et al., J/ψ elliptic flow in Pb-Pb collisions at $\sqrt{s_{NN}} = 5.02$ TeV, *Phys. Rev. Lett.* 119 (24) (2017) 242301, arXiv:1709.05260 [nucl-ex].
- [20] P. Braun-Munzinger, J. Stachel, (Non)thermal aspects of charmonium production and a new look at J/ψ suppression, *Phys. Lett. B* 490 (2000) 196–202, arXiv:nucl-th/0007059 [nucl-th].
- [21] A. Andronic, P. Braun-Munzinger, K. Redlich, J. Stachel, Evidence for charmonium generation at the phase boundary in ultra-relativistic nuclear collisions, *Phys. Lett. B* 652 (2007) 259–261, arXiv:nucl-th/0701079 [NUCL-TH].
- [22] R.L. Thews, M. Schroedter, J. Rafelski, Enhanced J/ψ production in deconfined quark matter, *Phys. Rev. C* 63 (2001) 054905, arXiv:hep-ph/0007323 [hep-ph].
- [23] E.G. Ferreira, Charmonium dissociation and recombination at LHC: revisiting comovers, *Phys. Lett. B* 731 (2014) 57–63, arXiv:1210.3209 [hep-ph].
- [24] X. Zhao, R. Rapp, Transverse momentum spectra of J/ψ in heavy-ion collisions, *Phys. Lett. B* 664 (2008) 253–257, arXiv:0712.2407 [hep-ph].
- [25] K. Zhou, N. Xu, Z. Xu, P. Zhuang, Medium effects on charmonium production at ultrarelativistic energies available at the CERN Large Hadron Collider, *Phys. Rev. C* 89 (5) (2014) 054911, arXiv:1401.5845 [nucl-th].
- [26] N. Armesto, Nuclear shadowing, *J. Phys. G* 32 (2006) R367–R394, arXiv:hep-ph/0604108 [hep-ph].
- [27] ALICE Collaboration, S. Acharya, et al., Inclusive J/ψ production at mid-rapidity in pp collisions at $\sqrt{s} = 5.02$ TeV, *J. High Energy Phys.* 10 (2019) 084, arXiv:1905.07211 [nucl-ex].
- [28] ALICE Collaboration, J. Adam, et al., Inclusive, prompt and non-prompt J/ψ production at mid-rapidity in Pb-Pb collisions at $\sqrt{s_{NN}} = 2.76$ TeV, *J. High Energy Phys.* 07 (2015) 051, arXiv:1504.07151 [nucl-ex].
- [29] ALICE Collaboration, J. Adam, et al., J/ψ suppression at forward rapidity in Pb-Pb collisions at $\sqrt{s_{NN}} = 5.02$ TeV, *Phys. Lett. B* 766 (2017) 212–224, arXiv:1606.08197 [nucl-ex].
- [30] ATLAS Collaboration, M. Aaboud, et al., Prompt and non-prompt J/ψ and $\psi(2S)$ suppression at high transverse momentum in 5.02 TeV Pb-Pb collisions with the ATLAS experiment, arXiv:1805.04077 [nucl-ex].
- [31] CMS Collaboration, A.M. Sirunyan, et al., Measurement of prompt and non-prompt charmonium suppression in Pb-Pb collisions at 5.02 TeV, *Eur. Phys. J. C* (2017), arXiv:1712.08959 [nucl-ex].
- [32] ALICE Collaboration, S. Acharya, et al., Inclusive J/ψ production in Xe-Xe collisions at $\sqrt{s_{NN}} = 5.44$ TeV, *Phys. Lett. B* 785 (2018) 419–428, arXiv:1805.04383 [nucl-ex].

- [33] ALICE Collaboration, K. Aamodt, et al., The ALICE experiment at the CERN LHC, *J. Instrum.* 3 (2008) S08002.
- [34] ALICE Collaboration, B. Abelev, et al., Performance of the ALICE experiment at the CERN LHC, *Int. J. Mod. Phys. A* 29 (2014) 1430044, arXiv:1402.4476 [nucl-ex].
- [35] ALICE Collaboration, K. Aamodt, et al., Alignment of the ALICE inner tracking system with cosmic-ray tracks, *J. Instrum.* 5 (2010) P03003, arXiv:1001.0502 [physics.ins-det].
- [36] ALICE Collaboration, J. Alme, et al., The ALICE TPC, a large 3-dimensional tracking device with fast readout for ultra-high multiplicity events, *Nucl. Instrum. Methods A* 622 (2010) 316–367, arXiv:1001.1950 [physics.ins-det].
- [37] ALICE Collaboration, E. Abbas, et al., Performance of the ALICE VZERO system, *J. Instrum.* 8 (2013) P10016, arXiv:1306.3130 [nucl-ex].
- [38] ALICE Collaboration, B. Abelev, et al., Centrality determination of Pb-Pb collisions at $\sqrt{s_{NN}} = 2.76$ TeV with ALICE, *Phys. Rev. C* 88 (4) (2013) 044909, arXiv:1301.4361 [nucl-ex].
- [39] ALICE Collaboration, J. Adam, et al., Centrality dependence of the charged-particle multiplicity density at midrapidity in Pb-Pb collisions at $\sqrt{s_{NN}} = 5.02$ TeV, *Phys. Rev. Lett.* 116 (22) (2016) 222302, arXiv:1512.06104 [nucl-ex].
- [40] ALICE Collaboration, Centrality determination in heavy ion collisions, ALICE-PUBLIC-2018-011, <http://cds.cern.ch/record/2636623>, 2018.
- [41] ALICE Collaboration, G. Puddu, et al., The zero degree calorimeters for the ALICE experiment, *Nucl. Instrum. Methods Phys. Res., Sect. A* 581 (2007) 397–401.
- [42] Particle Data Group Collaboration, C. Patrignani, et al., Review of particle physics, *Chin. Phys. C* 40 (10) (2016) 100001.
- [43] X.-N. Wang, M. Gyulassy, HIJING: a Monte Carlo model for multiple jet production in pp, pA and AA collisions, *Phys. Rev. D* 44 (1991) 3501–3516.
- [44] P. Golonka, Z. Was, PHOTOS Monte Carlo: a precision tool for QED corrections in Z and W decays, *Eur. Phys. J. C* 45 (2006) 97, arXiv:hep-ph/0506026 [hep-ph].
- [45] R. Brun, F. Bruyant, M. Maire, A.C. McPherson, P. Zanzanini, GEANT 3: User's Guide Geant 3.10, Geant 3.11; rev. version, CERN, Geneva, 1987, <https://cds.cern.ch/record/1119728>.
- [46] ALICE Collaboration, J. Adam, et al., Measurement of an excess in the yield of J/ψ at very low p_T in Pb-Pb collisions at $\sqrt{s_{NN}} = 2.76$ TeV, *Phys. Rev. Lett.* 116 (22) (2016) 222301, arXiv:1509.08802 [nucl-ex].
- [47] ALICE Collaboration, E. Abbas, et al., Charmonium and e^+e^- pair photoproduction at mid-rapidity in ultra-peripheral Pb-Pb collisions at $\sqrt{s_{NN}} = 2.76$ TeV, *Eur. Phys. J. C* 73 (11) (2013) 2617, arXiv:1305.1467 [nucl-ex].
- [48] R. Barlow, Systematic errors: facts and fictions, arXiv:hep-ex/0207026.
- [49] A. Andronic, P. Braun-Munzinger, M.K. Koehler, K. Redlich, J. Stachel, Transverse momentum distributions of charmonium states with the statistical hadronization model, *Phys. Lett. B* 797 (2019) 134836, arXiv:1901.09200 [nucl-th].
- [50] A. Capella, A. Kaidalov, A. Kouider Akil, C. Gerschel, J/ψ and $\psi(2S)$ suppression in heavy-ion collisions, *Phys. Lett. B* 393 (1997) 431–436, arXiv:hep-ph/9607265 [hep-ph].
- [51] B. Schenke, S. Jeon, C. Gale, (3+1) D hydrodynamic simulation of relativistic heavy-ion collisions, *Phys. Rev. C* 82 (2010) 014903, arXiv:1004.1408 [hep-ph].
- [52] W. Florkowski, Phenomenology of Ultra-Relativistic Heavy-Ion Collisions, World Scientific Publishing Co. Pte. Ltd., 2010.
- [53] ALICE Collaboration, S. Acharya, et al., Studies of J/ψ production at forward rapidity in Pb-Pb collisions at $\sqrt{s_{NN}} = 5.02$ TeV, arXiv:1909.03158 [nucl-ex].
- [54] NA50 Collaboration, M.C. Abreu, et al., Transverse momentum distributions of J/ψ , $\psi(2S)$, Drell-Yan and continuum dimuons produced in Pb-Pb interactions at the SPS, *Phys. Lett. B* 499 (2001) 85–96.
- [55] PHENIX Collaboration, A. Adare, et al., Ground and excited charmonium state production in $p+p$ collisions at $\sqrt{s} = 200$ GeV, *Phys. Rev. D* 85 (2012) 092004, arXiv:1105.1966 [hep-ex].
- [56] PHENIX Collaboration, A. Adare, et al., J/ψ production in $\sqrt{s_{NN}} = 200$ -GeV Cu+Cu collisions, *Phys. Rev. Lett.* 101 (2008) 122301, arXiv:0801.0220 [nucl-ex].
- [57] X. Zhao, R. Rapp, Medium modifications and production of charmonia at LHC, *Nucl. Phys. A* 859 (2011) 114–125, arXiv:1102.2194 [hep-ph].
- [58] X. Du, R. Rapp, Sequential regeneration of charmonia in heavy-ion collisions, *Nucl. Phys. A* 943 (2015) 147–158, arXiv:1504.00670 [hep-ph].
- [59] J.W. Cronin, H.J. Frisch, M.J. Shochet, J.P. Boymond, R. Mermod, P.A. Piroué, R.L. Sumner, Production of hadrons with large transverse momentum at 200, 300, and 400 GeV, *Phys. Rev. D* 11 (1975) 3105–3123.s

ALICE Collaboration

S. Acharya¹⁴¹, D. Adamová⁹⁴, A. Adler⁷⁴, J. Adolfsson⁸⁰, M.M. Aggarwal⁹⁹, G. Aglieri Rinella³³, M. Agnello³⁰, N. Agrawal^{10,53}, Z. Ahammed¹⁴¹, S. Ahmad¹⁶, S.U. Ahn⁷⁶, A. Akindinov⁹¹, M. Al-Turany¹⁰⁶, S.N. Alam¹⁴¹, D.S.D. Albuquerque¹²², D. Aleksandrov⁸⁷, B. Alessandro⁵⁸, H.M. Alfanda⁶, R. Alfaro Molina⁷¹, B. Ali¹⁶, Y. Ali¹⁴, A. Alici^{10,26,53}, A. Alkin², J. Alme²¹, T. Alt⁶⁸, L. Altenkamper²¹, I. Altsybeev¹¹², M.N. Anaam⁶, C. Andrei⁴⁷, D. Andreou³³, H.A. Andrews¹¹⁰, A. Andronic¹⁴⁴, M. Angeletti³³, V. Anguelov¹⁰³, C. Anson¹⁵, T. Antičić¹⁰⁷, F. Antinori⁵⁶, P. Antonioli⁵³, R. Anwar¹²⁵, N. Apadula⁷⁹, L. Aphecetche¹¹⁴, H. Appelshäuser⁶⁸, S. Arcelli²⁶, R. Arnaldi⁵⁸, M. Arratia⁷⁹, I.C. Arsene²⁰, M. Arslanok¹⁰³, A. Augustinus³³, R. Averbeck¹⁰⁶, S. Aziz⁶¹, M.D. Azmi¹⁶, A. Badalà⁵⁵, Y.W. Baek⁴⁰, S. Bagnasco⁵⁸, X. Bai¹⁰⁶, R. Bailhache⁶⁸, R. Bala¹⁰⁰, A. Baldisseri¹³⁷, M. Ball⁴², S. Balouza¹⁰⁴, R. Barbera²⁷, L. Barioglio²⁵, G.G. Barnaföldi¹⁴⁵, L.S. Barnby⁹³, V. Barret¹³⁴, P. Bartalini⁶, K. Barth³³, E. Bartsch⁶⁸, F. Baruffaldi²⁸, N. Bastid¹³⁴, S. Basu¹⁴³, G. Batigne¹¹⁴, B. Batyunya⁷⁵, D. Bauri⁴⁸, J.L. Bazo Alba¹¹¹, I.G. Bearden⁸⁸, C. Bedda⁶³, N.K. Behera⁶⁰, I. Belikov¹³⁶, A.D.C. Bell Hechavarria¹⁴⁴, F. Bellini³³, R. Bellwied¹²⁵, V. Belyaev⁹², G. Bencedi¹⁴⁵, S. Beole²⁵, A. Bercuci⁴⁷, Y. Berdnikov⁹⁷, D. Berenyi¹⁴⁵, R.A. Bertens¹³⁰, D. Berzano⁵⁸, M.G. Besoiu⁶⁷, L. Betev³³, A. Bhasin¹⁰⁰, I.R. Bhat¹⁰⁰, M.A. Bhat³, H. Bhatt⁴⁸, B. Bhattacharjee⁴¹, A. Bianchi²⁵, L. Bianchi²⁵, N. Bianchi⁵¹, J. Bielčik³⁶, J. Bielčíková⁹⁴, A. Bilandzic^{104,117}, G. Biro¹⁴⁵, R. Biswas³, S. Biswas³, J.T. Blair¹¹⁹, D. Blau⁸⁷, C. Blume⁶⁸, G. Boca¹³⁹, F. Bock^{33,95}, A. Bogdanov⁹², S. Boi²³, L. Boldizsár¹⁴⁵, A. Bolozdynya⁹², M. Bombara³⁷, G. Bonomi¹⁴⁰, H. Borel¹³⁷, A. Borissov^{92,144}, H. Bossi¹⁴⁶, E. Botta²⁵, L. Bratrud⁶⁸, P. Braun-Munzinger¹⁰⁶, M. Bregant¹²¹, M. Broz³⁶, E.J. Brucken⁴³, E. Bruna⁵⁸, G.E. Bruno¹⁰⁵, M.D. Buckland¹²⁷, D. Budnikov¹⁰⁸, H. Buesching⁶⁸, S. Bufalino³⁰, O. Bugnon¹¹⁴, P. Buhler¹¹³, P. Buncic³³, Z. Buthelezi^{72,131}, J.B. Butt¹⁴, J.T. Buxton⁹⁶, S.A. Bysiak¹¹⁸, D. Caffarri⁸⁹, A. Caliva¹⁰⁶, E. Calvo Villar¹¹¹, R.S. Camacho⁴⁴, P. Camerini²⁴, A.A. Capon¹¹³, F. Carnesecchi^{10,26}, R. Caron¹³⁷, J. Castillo Castellanos¹³⁷, A.J. Castro¹³⁰, E.A.R. Casula⁵⁴, F. Catalano³⁰, C. Ceballos Sanchez⁵², P. Chakraborty⁴⁸, S. Chandra¹⁴¹, W. Chang⁶, S. Chapeland³³, M. Chartier¹²⁷, S. Chattopadhyay¹⁴¹, S. Chattopadhyay¹⁰⁹, A. Chauvin²³, C. Cheshkov¹³⁵, B. Cheynis¹³⁵, V. Chibante Barroso³³, D.D. Chinellato¹²², S. Cho⁶⁰, P. Chochula³³, T. Chowdhury¹³⁴, P. Christakoglou⁸⁹, C.H. Christensen⁸⁸, P. Christiansen⁸⁰, T. Chujo¹³³, C. Cicalo⁵⁴, L. Cifarelli^{10,26}, F. Cindolo⁵³,

J. Cleymans¹²⁴, F. Colamaria⁵², D. Colella⁵², A. Collu⁷⁹, M. Colocci²⁶, M. Concas^{58,ii},
G. Conesa Balbastre⁷⁸, Z. Conesa del Valle⁶¹, G. Contin^{24,127}, J.G. Contreras³⁶, T.M. Cormier⁹⁵,
Y. Corrales Morales²⁵, P. Cortese³¹, M.R. Cosentino¹²³, F. Costa³³, S. Costanza¹³⁹, P. Crochet¹³⁴,
E. Cuautle⁶⁹, P. Cui⁶, L. Cunqueiro⁹⁵, D. Dabrowski¹⁴², T. Dahms^{104,117}, A. Dainese⁵⁶,
F.P.A. Damas^{114,137}, M.C. Danisch¹⁰³, A. Danu⁶⁷, D. Das¹⁰⁹, I. Das¹⁰⁹, P. Das⁸⁵, P. Das³, S. Das³,
A. Dash⁸⁵, S. Dash⁴⁸, S. De⁸⁵, A. De Caro²⁹, G. de Cataldo⁵², J. de Cuveland³⁸, A. De Falco²³,
D. De Gruttola¹⁰, N. De Marco⁵⁸, S. De Pasquale²⁹, S. Deb⁴⁹, B. Debjani³, H.F. Degenhardt¹²¹,
K.R. Deja¹⁴², A. Deloff⁸⁴, S. Delsanto^{25,131}, D. Devetak¹⁰⁶, P. Dhankher⁴⁸, D. Di Bari³², A. Di Mauro³³,
R.A. Diaz⁸, T. Dietel¹²⁴, P. Dillenseger⁶⁸, Y. Ding⁶, R. Divià³³, D.U. Dixit¹⁹, Ø. Djuvsland²¹,
U. Dmitrieva⁶², A. Dobrin^{33,67}, B. Dönigus⁶⁸, O. Dordic²⁰, A.K. Dubey¹⁴¹, A. Dubla¹⁰⁶, S. Dudi⁹⁹,
M. Dukhishyam⁸⁵, P. Dupieux¹³⁴, R.J. Ehlers¹⁴⁶, V.N. Eikeland²¹, D. Elia⁵², H. Engel⁷⁴, E. Epple¹⁴⁶,
B. Erazmus¹¹⁴, F. Erhardt⁹⁸, A. Erokhin¹¹², M.R. Ersdal²¹, B. Espagnon⁶¹, G. Eulisse³³, D. Evans¹¹⁰,
S. Evdokimov⁹⁰, L. Fabbietti^{104,117}, M. Faggin²⁸, J. Faivre⁷⁸, F. Fan⁶, A. Fantoni⁵¹, M. Fasel⁹⁵,
P. Fecchio³⁰, A. Feliciello⁵⁸, G. Feofilov¹¹², A. Fernández Téllez⁴⁴, A. Ferrero¹³⁷, A. Ferretti²⁵,
A. Festanti³³, V.J.G. Feuillard¹⁰³, J. Figiel¹¹⁸, S. Filchagin¹⁰⁸, D. Finogeev⁶², F.M. Fionda²¹, G. Fiorenza⁵²,
F. Flor¹²⁵, S. Foertsch⁷², P. Foka¹⁰⁶, S. Fokin⁸⁷, E. Fragiaco⁵⁹, U. Frankendorf¹⁰⁶, U. Fuchs³³,
C. Furget⁷⁸, A. Furs⁶², M. Fusco Girard²⁹, J.J. Gaardhøje⁸⁸, M. Gagliardi²⁵, A.M. Gago¹¹¹, A. Gal¹³⁶,
C.D. Galvan¹²⁰, P. Ganoti⁸³, C. Garabatos¹⁰⁶, E. Garcia-Solis¹¹, K. Garg²⁷, C. Gargiulo³³, A. Garibli⁸⁶,
K. Garner¹⁴⁴, P. Gasik^{104,117}, E.F. Gauger¹¹⁹, M.B. Gay Ducati⁷⁰, M. Germain¹¹⁴, J. Ghosh¹⁰⁹,
P. Ghosh¹⁴¹, S.K. Ghosh³, P. Gianotti⁵¹, P. Giubellino^{58,106}, P. Giubilato²⁸, P. Glässel¹⁰³,
D.M. Gómez Coral⁷¹, A. Gomez Ramirez⁷⁴, V. Gonzalez¹⁰⁶, P. González-Zamora⁴⁴, S. Gorbunov³⁸,
L. Görlich¹¹⁸, S. Gotovac³⁴, V. Grabski⁷¹, L.K. Graczykowski¹⁴², K.L. Graham¹¹⁰, L. Greiner⁷⁹, A. Grelli⁶³,
C. Grigoras³³, V. Grigoriev⁹², A. Grigoryan¹, S. Grigoryan⁷⁵, O.S. Groettkvik²¹, F. Grosa³⁰,
J.F. Grosse-Oetringhaus³³, R. Grosso¹⁰⁶, R. Guernane⁷⁸, M. Guittiere¹¹⁴, K. Gulbrandsen⁸⁸, T. Gunji¹³²,
A. Gupta¹⁰⁰, R. Gupta¹⁰⁰, I.B. Guzman⁴⁴, R. Haake¹⁴⁶, M.K. Habib¹⁰⁶, C. Hadjidakis⁶¹, H. Hamagaki⁸¹,
G. Hamar¹⁴⁵, M. Hamid⁶, R. Hannigan¹¹⁹, M.R. Haque^{63,85}, A. Harlanderova¹⁰⁶, J.W. Harris¹⁴⁶,
A. Harton¹¹, J.A. Hasenbichler³³, H. Hassan⁹⁵, D. Hatzifotiadou^{10,53}, P. Hauer⁴², S. Hayashi¹³²,
S.T. Heckel^{68,104}, E. Hellbär⁶⁸, H. Helstrup³⁵, A. Herghelegiu⁴⁷, T. Herman³⁶, E.G. Hernandez⁴⁴,
G. Herrera Corral⁹, F. Herrmann¹⁴⁴, K.F. Hetland³⁵, T.E. Hilden⁴³, H. Hillemanns³³, C. Hills¹²⁷,
B. Hippolyte¹³⁶, B. Hohlweger¹⁰⁴, D. Horak³⁶, A. Hornung⁶⁸, S. Hornung¹⁰⁶, R. Hosokawa^{15,133},
P. Hristov³³, C. Huang⁶¹, C. Hughes¹³⁰, P. Huhn⁶⁸, T.J. Humanic⁹⁶, H. Hushnud¹⁰⁹, L.A. Husova¹⁴⁴,
N. Hussain⁴¹, S.A. Hussain¹⁴, D. Hutter³⁸, J.P. Iddon^{33,127}, R. Ilkaev¹⁰⁸, M. Inaba¹³³, G.M. Innocenti³³,
M. Ippolitov⁸⁷, A. Isakov⁹⁴, M.S. Islam¹⁰⁹, M. Ivanov¹⁰⁶, V. Ivanov⁹⁷, V. Izucheev⁹⁰, B. Jacak⁷⁹,
N. Jacazio⁵³, P.M. Jacobs⁷⁹, S. Jadlovská¹¹⁶, J. Jadlovsky¹¹⁶, S. Jaelani⁶³, C. Jahnke¹²¹,
M.J. Jakubowska¹⁴², M.A. Janik¹⁴², T. Janson⁷⁴, M. Jercic⁹⁸, O. Jevons¹¹⁰, R.T. Jimenez Bustamante¹⁰⁶,
M. Jin¹²⁵, F. Jonas^{95,144}, P.G. Jones¹¹⁰, J. Jung⁶⁸, M. Jung⁶⁸, A. Jusko¹¹⁰, P. Kalinak⁶⁴, A. Kalweit³³,
V. Kaplin⁹², S. Kar⁶, A. Karasu Uysal⁷⁷, O. Karavichev⁶², T. Karavicheva⁶², P. Karczmarczyk³³,
E. Karpechev⁶², A. Kazantsev⁸⁷, U. Keschull⁷⁴, R. Keidel⁴⁶, M. Keil³³, B. Ketzer⁴², Z. Khabanova⁸⁹,
A.M. Khan⁶, S. Khan¹⁶, S.A. Khan¹⁴¹, A. Khanzadeev⁹⁷, Y. Kharlov⁹⁰, A. Khatun¹⁶, A. Khuntia¹¹⁸,
B. Kileng³⁵, B. Kim⁶⁰, B. Kim¹³³, D. Kim¹⁴⁷, D.J. Kim¹²⁶, E.J. Kim⁷³, H. Kim^{17,147}, J. Kim¹⁴⁷, J.S. Kim⁴⁰,
J. Kim¹⁰³, J. Kim¹⁴⁷, J. Kim⁷³, M. Kim¹⁰³, S. Kim¹⁸, T. Kim¹⁴⁷, T. Kim¹⁴⁷, S. Kirsch^{38,68}, I. Kisel³⁸,
S. Kiselev⁹¹, A. Kisel¹⁴², J.L. Klay⁵, C. Klein⁶⁸, J. Klein⁵⁸, S. Klein⁷⁹, C. Klein-Bösing¹⁴⁴, M. Kleiner⁶⁸,
A. Kluge³³, M.L. Knichel³³, A.G. Knospe¹²⁵, C. Kobdaj¹¹⁵, M.K. Köhler¹⁰³, T. Kollegger¹⁰⁶,
A. Kondratyev⁷⁵, N. Kondratyeva⁹², E. Kondratyuk⁹⁰, J. König⁶⁸, P.J. Konopka³³, L. Koska¹¹⁶,
O. Kovalenko⁸⁴, V. Kovalenko¹¹², M. Kowalski¹¹⁸, I. Králik⁶⁴, A. Kravčáková³⁷, L. Kreis¹⁰⁶,
M. Krivda^{64,110}, F. Krizek⁹⁴, K. Krizkova Gajdosova³⁶, M. Krüger⁶⁸, E. Kryshen⁹⁷, M. Krzewicki³⁸,
A.M. Kubera⁹⁶, V. Kučera⁶⁰, C. Kuhn¹³⁶, P.G. Kuijper⁸⁹, L. Kumar⁹⁹, S. Kumar⁴⁸, S. Kundu⁸⁵,
P. Kurashvili⁸⁴, A. Kurepin⁶², A.B. Kurepin⁶², A. Kuryakin¹⁰⁸, S. Kushpil⁹⁴, J. Kvapil¹¹⁰, M.J. Kweon⁶⁰,
J.Y. Kwon⁶⁰, Y. Kwon¹⁴⁷, S.L. La Pointe³⁸, P. La Rocca²⁷, Y.S. Lai⁷⁹, R. Langoy¹²⁹, K. Lapidus³³,
A. Lardeux²⁰, P. Larionov⁵¹, E. Laudi³³, R. Lavicka³⁶, T. Lazareva¹¹², R. Lea²⁴, L. Leardini¹⁰³, J. Lee¹³³,
S. Lee¹⁴⁷, F. Lehas⁸⁹, S. Lehner¹¹³, J. Lehrbach³⁸, R.C. Lemmon⁹³, I. León Monzón¹²⁰, E.D. Lesser¹⁹,
M. Lettrich³³, P. Lévai¹⁴⁵, X. Li¹², X.L. Li⁶, J. Lien¹²⁹, R. Lietava¹¹⁰, B. Lim¹⁷, V. Lindenstruth³⁸,
S.W. Lindsay¹²⁷, C. Lippmann¹⁰⁶, M.A. Lisa⁹⁶, V. Litichevskiy⁴³, A. Liu¹⁹, S. Liu⁹⁶, W.J. Llope¹⁴³,

I.M. Lofnes²¹, V. Loginov⁹², C. Loizides⁹⁵, P. Loncar³⁴, X. Lopez¹³⁴, E. López Torres⁸, J.R. Luhder¹⁴⁴, M. Lunardon²⁸, G. Luparello⁵⁹, Y. Ma³⁹, A. Maevskaya⁶², M. Mager³³, S.M. Mahmood²⁰, T. Mahmoud⁴², A. Maire¹³⁶, R.D. Majka¹⁴⁶, M. Malaev⁹⁷, Q.W. Malik²⁰, L. Malinina^{75,iii}, D. Mal'Kevich⁹¹, P. Malzacher¹⁰⁶, G. Mandaglio⁵⁵, V. Manko⁸⁷, F. Manso¹³⁴, V. Manzari⁵², Y. Mao⁶, M. Marchisone¹³⁵, J. Mareš⁶⁶, G.V. Margagliotti²⁴, A. Margotti⁵³, J. Margutti⁶³, A. Marín¹⁰⁶, C. Markert¹¹⁹, M. Marquard⁶⁸, N.A. Martin¹⁰³, P. Martinengo³³, J.L. Martinez¹²⁵, M.I. Martínez⁴⁴, G. Martínez García¹¹⁴, M. Martinez Pedreira³³, S. Masciocchi¹⁰⁶, M. Maserà²⁵, A. Masoni⁵⁴, L. Massacrier⁶¹, E. Masson¹¹⁴, A. Mastroserio^{52,138}, A.M. Mathis^{104,117}, O. Matonoha⁸⁰, P.F.T. Matuoka¹²¹, A. Matyja¹¹⁸, C. Mayer¹¹⁸, M. Mazzilli⁵², M.A. Mazzoni⁵⁷, A.F. Mechler⁶⁸, F. Meddi²², Y. Melikyan^{62,92}, A. Menchaca-Rocha⁷¹, C. Mengke⁶, E. Meninno^{29,113}, M. Meres¹³, S. Mhlanga¹²⁴, Y. Miake¹³³, L. Micheletti²⁵, D.L. Mihaylov¹⁰⁴, K. Mikhaylov^{75,91}, A. Mischke^{63,i}, A.N. Mishra⁶⁹, D. Miśkowiec¹⁰⁶, A. Modak³, N. Mohammadi³³, A.P. Mohanty⁶³, B. Mohanty⁸⁵, M. Mohisin Khan^{16,iv}, C. Mordasini¹⁰⁴, D.A. Moreira De Godoy¹⁴⁴, L.A.P. Moreno⁴⁴, I. Morozov⁶², A. Morsch³³, T. Mrnjavac³³, V. Muccifora⁵¹, E. Mudnic³⁴, D. Mühlheim¹⁴⁴, S. Muhuri¹⁴¹, J.D. Mulligan⁷⁹, M.G. Munhoz¹²¹, R.H. Munzer⁶⁸, H. Murakami¹³², S. Murray¹²⁴, L. Musa³³, J. Musinsky⁶⁴, C.J. Myers¹²⁵, J.W. Myrcha¹⁴², B. Naik⁴⁸, R. Nair⁸⁴, B.K. Nandi⁴⁸, R. Nania^{10,53}, E. Nappi⁵², M.U. Naru¹⁴, A.F. Nassirpour⁸⁰, C. Nattrass¹³⁰, R. Nayak⁴⁸, T.K. Nayak⁸⁵, S. Nazarenko¹⁰⁸, A. Neagu²⁰, R.A. Negrao De Oliveira⁶⁸, L. Nellen⁶⁹, S.V. Nesbo³⁵, G. Neskovic³⁸, D. Nesterov¹¹², L.T. Neumann¹⁴², B.S. Nielsen⁸⁸, S. Nikolaev⁸⁷, S. Nikulin⁸⁷, V. Nikulin⁹⁷, F. Noferini^{10,53}, P. Nomokonov⁷⁵, J. Norman^{78,127}, N. Novitzky¹³³, P. Nowakowski¹⁴², A. Nyanin⁸⁷, J. Nystrand²¹, M. Ogino⁸¹, A. Ohlson^{80,103}, J. Oleniacz¹⁴², A.C. Oliveira Da Silva^{121,130}, M.H. Oliver¹⁴⁶, C. Oppedisano⁵⁸, R. Orava⁴³, A. Ortiz Velasquez⁶⁹, A. Oskarsson⁸⁰, J. Otwinowski¹¹⁸, K. Oyama⁸¹, Y. Pachmayer¹⁰³, V. Pacik⁸⁸, D. Pagano¹⁴⁰, G. Paić⁶⁹, J. Pan¹⁴³, A.K. Pandey⁴⁸, S. Panebianco¹³⁷, P. Pareek^{49,141}, J. Park⁶⁰, J.E. Parkkila¹²⁶, S. Parmar⁹⁹, S.P. Pathak¹²⁵, R.N. Patra¹⁴¹, B. Paul^{23,58}, H. Pei⁶, T. Peitzmann⁶³, X. Peng⁶, L.G. Pereira⁷⁰, H. Pereira Da Costa¹³⁷, D. Peresunko⁸⁷, G.M. Perez⁸, E. Perez Lezama⁶⁸, V. Peskov⁶⁸, Y. Pestov⁴, V. Petráček³⁶, M. Petrovici⁴⁷, R.P. Pezzi⁷⁰, S. Piano⁵⁹, M. Pikna¹³, P. Pillot¹¹⁴, O. Pinazza^{33,53}, L. Pinsky¹²⁵, C. Pinto²⁷, S. Pisano^{10,51}, D. Pistone⁵⁵, M. Płoskoń⁷⁹, M. Planinic⁹⁸, F. Pliquett⁶⁸, J. Pluta¹⁴², S. Pochybova^{145,i}, M.G. Poghosyan⁹⁵, B. Polichtchouk⁹⁰, N. Poljak⁹⁸, A. Pop⁴⁷, H. Poppenborg¹⁴⁴, S. Porteboeuf-Houssais¹³⁴, V. Pozdniakov⁷⁵, S.K. Prasad³, R. Preghenella⁵³, F. Prino⁵⁸, C.A. Pruneau¹⁴³, I. Pshenichnov⁶², M. Puccio^{25,33}, J. Putschke¹⁴³, R.E. Quishpe¹²⁵, S. Ragoni¹¹⁰, S. Raha³, S. Rajput¹⁰⁰, J. Rak¹²⁶, A. Rakotozafindrabe¹³⁷, L. Ramello³¹, F. Rami¹³⁶, R. Raniwala¹⁰¹, S. Raniwala¹⁰¹, S.S. Räsänen⁴³, R. Rath⁴⁹, V. Ratza⁴², I. Ravasenga^{30,89}, K.F. Read^{95,130}, K. Redlich^{84,v}, A. Rehman²¹, P. Reichelt⁶⁸, F. Reidt³³, X. Ren⁶, R. Renfordt⁶⁸, Z. Rescakova³⁷, J.-P. Revol¹⁰, K. Reygers¹⁰³, V. Riabov⁹⁷, T. Richert^{80,88}, M. Richter²⁰, P. Riedler³³, W. Riegler³³, F. Riggi²⁷, C. Ristea⁶⁷, S.P. Rode⁴⁹, M. Rodríguez Cahuantzi⁴⁴, K. Røed²⁰, R. Rogalev⁹⁰, E. Rogochaya⁷⁵, D. Rohr³³, D. Röhrich²¹, P.S. Rokita¹⁴², F. Ronchetti⁵¹, E.D. Rosas⁶⁹, K. Roslon¹⁴², A. Rossi^{28,56}, A. Rotondi¹³⁹, A. Roy⁴⁹, P. Roy¹⁰⁹, O.V. Rueda⁸⁰, R. Rui²⁴, B. Rumyantsev⁷⁵, A. Rustamov⁸⁶, E. Ryabinkin⁸⁷, Y. Ryabov⁹⁷, A. Rybicki¹¹⁸, H. Rytkonen¹²⁶, O.A.M. Saarimaki⁴³, S. Sadhu¹⁴¹, S. Sadovsky⁹⁰, K. Šafařík³⁶, S.K. Saha¹⁴¹, B. Sahoo⁴⁸, P. Sahoo^{48,49}, R. Sahoo⁴⁹, S. Sahoo⁶⁵, P.K. Sahu⁶⁵, J. Saini¹⁴¹, S. Sakai¹³³, S. Sambyal¹⁰⁰, V. Samsonov^{92,97}, D. Sarkar¹⁴³, N. Sarkar¹⁴¹, P. Sarma⁴¹, V.M. Sarti¹⁰⁴, M.H.P. Sas⁶³, E. Scapparone⁵³, B. Schaefer⁹⁵, J. Schambach¹¹⁹, H.S. Scheid⁶⁸, C. Schiaua⁴⁷, R. Schicker¹⁰³, A. Schmah¹⁰³, C. Schmidt¹⁰⁶, H.R. Schmidt¹⁰², M.O. Schmidt¹⁰³, M. Schmidt¹⁰², N.V. Schmidt^{68,95}, A.R. Schmier¹³⁰, J. Schukraft⁸⁸, Y. Schutz^{33,136}, K. Schwarz¹⁰⁶, K. Schweda¹⁰⁶, G. Scioli²⁶, E. Scomparin⁵⁸, M. Šefčík³⁷, J.E. Seger¹⁵, Y. Sekiguchi¹³², D. Sekihata¹³², I. Selyuzhenkov^{92,106}, S. Senyukov¹³⁶, D. Serebryakov⁶², E. Serradilla⁷¹, A. Sevcenco⁶⁷, A. Shabanov⁶², A. Shabetai¹¹⁴, R. Shahoyan³³, W. Shaikh¹⁰⁹, A. Shangaraev⁹⁰, A. Sharma⁹⁹, A. Sharma¹⁰⁰, H. Sharma¹¹⁸, M. Sharma¹⁰⁰, N. Sharma⁹⁹, A.I. Sheikh¹⁴¹, K. Shigaki⁴⁵, M. Shimomura⁸², S. Shirinkin⁹¹, Q. Shou³⁹, Y. Sibiriak⁸⁷, S. Siddhanta⁵⁴, T. Siemiarczuk⁸⁴, D. Silvermyr⁸⁰, G. Simatovic⁸⁹, G. Simonetti^{33,104}, R. Singh⁸⁵, R. Singh¹⁰⁰, R. Singh⁴⁹, V.K. Singh¹⁴¹, V. Singhal¹⁴¹, T. Sinha¹⁰⁹, B. Sitar¹³, M. Sitta³¹, T.B. Skaali²⁰, M. Slupecki¹²⁶, N. Smirnov¹⁴⁶, R.J.M. Snellings⁶³, T.W. Snellman^{43,126}, C. Soncco¹¹¹, J. Song^{60,125}, A. Songmoolnak¹¹⁵, F. Soramel²⁸, S. Sorensen¹³⁰, I. Sputowska¹¹⁸, J. Stachel¹⁰³, I. Stan⁶⁷, P. Stankus⁹⁵, P.J. Steffanic¹³⁰, E. Stenlund⁸⁰, D. Stocco¹¹⁴, M.M. Storetvedt³⁵, L.D. Stritto²⁹, A.A.P. Suaide¹²¹, T. Sugitate⁴⁵, C. Suire⁶¹, M. Suleymanov¹⁴,

M. Suljic³³, R. Sultanov⁹¹, M. Šumbera⁹⁴, S. Sumowidagdo⁵⁰, S. Swain⁶⁵, A. Szabo¹³, I. Szarka¹³, U. Tabassam¹⁴, G. TAILLEPIED¹³⁴, J. Takahashi¹²², G.J. Tambave²¹, S. Tang^{6,134}, M. Tarhini¹¹⁴, M.G. Tarzila⁴⁷, A. Tauro³³, G. Tejada Muñoz⁴⁴, A. Telesca³³, C. Terrevoli¹²⁵, D. Thakur⁴⁹, S. Thakur¹⁴¹, D. Thomas¹¹⁹, F. Thoresen⁸⁸, R. Tieulent¹³⁵, A. Tikhonov⁶², A.R. Timmins¹²⁵, A. Toia⁶⁸, N. Topilskaya⁶², M. Toppi⁵¹, F. Torales-Acosta¹⁹, S.R. Torres^{9,120}, A. Trifiro⁵⁵, S. Tripathy⁴⁹, T. Tripathy⁴⁸, S. Trogolo²⁸, G. Trombetta³², L. Tropp³⁷, V. Trubnikov², W.H. Trzaska¹²⁶, T.P. Trzcinski¹⁴², B.A. Trzeciak⁶³, T. Tsuji¹³², A. Tumkin¹⁰⁸, R. Turrisi⁵⁶, T.S. Tveter²⁰, K. Ullaland²¹, E.N. Umaka¹²⁵, A. Uras¹³⁵, G.L. Usai²³, A. Utrobicic⁹⁸, M. Vala³⁷, N. Valle¹³⁹, S. Vallero⁵⁸, N. van der Kolk⁶³, L.V.R. van Doremalen⁶³, M. van Leeuwen⁶³, P. Vande Vyvre³³, D. Varga¹⁴⁵, Z. Varga¹⁴⁵, M. Varga-Kofarago¹⁴⁵, A. Vargas⁴⁴, M. Vasileiou⁸³, A. Vasiliev⁸⁷, O. Vázquez Doce^{104,117}, V. Vechernin¹¹², A.M. Veen⁶³, E. Vercellin²⁵, S. Vergara Limón⁴⁴, L. Vermunt⁶³, R. Vernet⁷, R. Vértesi¹⁴⁵, L. Vickovic³⁴, Z. Vilakazi¹³¹, O. Villalobos Baillie¹¹⁰, A. Villatoro Tello⁴⁴, G. VINO⁵², A. Vinogradov⁸⁷, T. Virgili²⁹, V. Vislavicius⁸⁸, A. Vodopyanov⁷⁵, B. Volkel³³, M.A. Völkl¹⁰², K. Voloshin⁹¹, S.A. Voloshin¹⁴³, G. Volpe³², B. von Haller³³, I. Vorobyev¹⁰⁴, D. Voscek¹¹⁶, J. Vrláková³⁷, B. Wagner²¹, M. Weber¹¹³, S.G. Weber¹⁴⁴, A. Wegrzynek³³, D.F. Weiser¹⁰³, S.C. Wenzel³³, J.P. Wessels¹⁴⁴, J. Wiechula⁶⁸, J. Wikne²⁰, G. Wilk⁸⁴, J. Wilkinson^{10,53}, G.A. Willems³³, E. Willsher¹¹⁰, B. Windelband¹⁰³, M. Winn¹³⁷, W.E. Witt¹³⁰, Y. Wu¹²⁸, R. Xu⁶, S. Yalcin⁷⁷, K. Yamakawa⁴⁵, S. Yang²¹, S. Yano¹³⁷, Z. Yin⁶, H. Yokoyama⁶³, I.-K. Yoo¹⁷, J.H. Yoon⁶⁰, S. Yuan²¹, A. Yuncu¹⁰³, V. Yurchenko², V. Zaccolo²⁴, A. Zaman¹⁴, C. Zampolli³³, H.J.C. Zanolli⁶³, N. Zardoshti³³, A. Zarochentsev¹¹², P. Závada⁶⁶, N. Zaviyalov¹⁰⁸, H. Zbroszczyk¹⁴², M. Zhalov⁹⁷, S. Zhang³⁹, X. Zhang⁶, Z. Zhang⁶, V. Zhrebchevskii¹¹², D. Zhou⁶, Y. Zhou⁸⁸, Z. Zhou²¹, J. Zhu^{6,106}, Y. Zhu⁶, A. Zichichi^{10,26}, M.B. Zimmermann³³, G. Zinovjev², N. Zurlo¹⁴⁰

¹ A.I. Alikhanyan National Science Laboratory (Yerevan Physics Institute) Foundation, Yerevan, Armenia

² Bogolyubov Institute for Theoretical Physics, National Academy of Sciences of Ukraine, Kiev, Ukraine

³ Bose Institute, Department of Physics and Centre for Astroparticle Physics and Space Science (CAPSS), Kolkata, India

⁴ Budker Institute for Nuclear Physics, Novosibirsk, Russia

⁵ California Polytechnic State University, San Luis Obispo, CA, United States

⁶ Central China Normal University, Wuhan, China

⁷ Centre de Calcul de l'IN2P3, Villeurbanne, Lyon, France

⁸ Centro de Aplicaciones Tecnológicas y Desarrollo Nuclear (CEADEN), Havana, Cuba

⁹ Centro de Investigación y de Estudios Avanzados (CINVESTAV), Mexico City and Mérida, Mexico

¹⁰ Centro Fermi - Museo Storico della Fisica e Centro Studi e Ricerche "Enrico Fermi", Rome, Italy

¹¹ Chicago State University, Chicago, IL, United States

¹² China Institute of Atomic Energy, Beijing, China

¹³ Comenius University Bratislava, Faculty of Mathematics, Physics and Informatics, Bratislava, Slovakia

¹⁴ COMSATS University Islamabad, Islamabad, Pakistan

¹⁵ Creighton University, Omaha, NE, United States

¹⁶ Department of Physics, Aligarh Muslim University, Aligarh, India

¹⁷ Department of Physics, Pusan National University, Pusan, Republic of Korea

¹⁸ Department of Physics, Sejong University, Seoul, Republic of Korea

¹⁹ Department of Physics, University of California, Berkeley, CA, United States

²⁰ Department of Physics, University of Oslo, Oslo, Norway

²¹ Department of Physics and Technology, University of Bergen, Bergen, Norway

²² Dipartimento di Fisica dell'Università 'La Sapienza' and Sezione INFN, Rome, Italy

²³ Dipartimento di Fisica dell'Università and Sezione INFN, Cagliari, Italy

²⁴ Dipartimento di Fisica dell'Università and Sezione INFN, Trieste, Italy

²⁵ Dipartimento di Fisica dell'Università and Sezione INFN, Turin, Italy

²⁶ Dipartimento di Fisica e Astronomia dell'Università and Sezione INFN, Bologna, Italy

²⁷ Dipartimento di Fisica e Astronomia dell'Università and Sezione INFN, Catania, Italy

²⁸ Dipartimento di Fisica e Astronomia dell'Università and Sezione INFN, Padova, Italy

²⁹ Dipartimento di Fisica 'E.R. Caianiello' dell'Università and Gruppo Collegato INFN, Salerno, Italy

³⁰ Dipartimento DISAT del Politecnico and Sezione INFN, Turin, Italy

³¹ Dipartimento di Scienze e Innovazione Tecnologica dell'Università del Piemonte Orientale and INFN Sezione di Torino, Alessandria, Italy

³² Dipartimento Interateneo di Fisica 'M. Merlin' and Sezione INFN, Bari, Italy

³³ European Organization for Nuclear Research (CERN), Geneva, Switzerland

³⁴ Faculty of Electrical Engineering, Mechanical Engineering and Naval Architecture, University of Split, Split, Croatia

³⁵ Faculty of Engineering and Science, Western Norway University of Applied Sciences, Bergen, Norway

³⁶ Faculty of Nuclear Sciences and Physical Engineering, Czech Technical University in Prague, Prague, Czech Republic

³⁷ Faculty of Science, P.J. Šafárik University, Košice, Slovakia

³⁸ Frankfurt Institute for Advanced Studies, Johann Wolfgang Goethe-Universität Frankfurt, Frankfurt, Germany

³⁹ Fudan University, Shanghai, China

⁴⁰ Gangneung-Wonju National University, Gangneung, Republic of Korea

⁴¹ Gauhati University, Department of Physics, Guwahati, India

⁴² Helmholtz-Institut für Strahlen- und Kernphysik, Rheinische Friedrich-Wilhelms-Universität Bonn, Bonn, Germany

⁴³ Helsinki Institute of Physics (HIP), Helsinki, Finland

⁴⁴ High Energy Physics Group, Universidad Autónoma de Puebla, Puebla, Mexico

⁴⁵ Hiroshima University, Hiroshima, Japan

⁴⁶ Hochschule Worms, Zentrum für Technologietransfer und Telekommunikation (ZIT), Worms, Germany

- 47 Horia Hulubei National Institute of Physics and Nuclear Engineering, Bucharest, Romania
- 48 Indian Institute of Technology Bombay (IIT), Mumbai, India
- 49 Indian Institute of Technology Indore, Indore, India
- 50 Indonesian Institute of Sciences, Jakarta, Indonesia
- 51 INFN, Laboratori Nazionali di Frascati, Frascati, Italy
- 52 INFN, Sezione di Bari, Bari, Italy
- 53 INFN, Sezione di Bologna, Bologna, Italy
- 54 INFN, Sezione di Cagliari, Cagliari, Italy
- 55 INFN, Sezione di Catania, Catania, Italy
- 56 INFN, Sezione di Padova, Padova, Italy
- 57 INFN, Sezione di Roma, Rome, Italy
- 58 INFN, Sezione di Torino, Turin, Italy
- 59 INFN, Sezione di Trieste, Trieste, Italy
- 60 Inha University, Incheon, Republic of Korea
- 61 Institut de Physique Nucléaire d'Orsay (IPNO), Institut National de Physique Nucléaire et de Physique des Particules (IN2P3/CNRS), Université de Paris-Sud, Université Paris-Saclay, Orsay, France
- 62 Institute for Nuclear Research, Academy of Sciences, Moscow, Russia
- 63 Institute for Subatomic Physics, Utrecht University/Nikhef, Utrecht, Netherlands
- 64 Institute of Experimental Physics, Slovak Academy of Sciences, Košice, Slovakia
- 65 Institute of Physics, Homi Bhabha National Institute, Bhubaneswar, India
- 66 Institute of Physics of the Czech Academy of Sciences, Prague, Czech Republic
- 67 Institute of Space Science (ISS), Bucharest, Romania
- 68 Institut für Kernphysik, Johann Wolfgang Goethe-Universität Frankfurt, Frankfurt, Germany
- 69 Instituto de Ciencias Nucleares, Universidad Nacional Autónoma de México, Mexico City, Mexico
- 70 Instituto de Física, Universidade Federal do Rio Grande do Sul (UFRGS), Porto Alegre, Brazil
- 71 Instituto de Física, Universidad Nacional Autónoma de México, Mexico City, Mexico
- 72 iThemba LABS, National Research Foundation, Somerset West, South Africa
- 73 Jeonbuk National University, Jeonju, Republic of Korea
- 74 Johann-Wolfgang-Goethe Universität Frankfurt Institut für Informatik, Fachbereich Informatik und Mathematik, Frankfurt, Germany
- 75 Joint Institute for Nuclear Research (JINR), Dubna, Russia
- 76 Korea Institute of Science and Technology Information, Daejeon, Republic of Korea
- 77 KTO Karatay University, Konya, Turkey
- 78 Laboratoire de Physique Subatomique et de Cosmologie, Université Grenoble-Alpes, CNRS-IN2P3, Grenoble, France
- 79 Lawrence Berkeley National Laboratory, Berkeley, CA, United States
- 80 Lund University Department of Physics, Division of Particle Physics, Lund, Sweden
- 81 Nagasaki Institute of Applied Science, Nagasaki, Japan
- 82 Nara Women's University (NWU), Nara, Japan
- 83 National and Kapodistrian University of Athens, School of Science, Department of Physics, Athens, Greece
- 84 National Centre for Nuclear Research, Warsaw, Poland
- 85 National Institute of Science Education and Research, Homi Bhabha National Institute, Jatni, India
- 86 National Nuclear Research Center, Baku, Azerbaijan
- 87 National Research Centre Kurchatov Institute, Moscow, Russia
- 88 Niels Bohr Institute, University of Copenhagen, Copenhagen, Denmark
- 89 Nikhef, National institute for subatomic physics, Amsterdam, Netherlands
- 90 NRC Kurchatov Institute IHEP, Protvino, Russia
- 91 NRC "Kurchatov Institute" - ITEP, Moscow, Russia
- 92 NRNU Moscow Engineering Physics Institute, Moscow, Russia
- 93 Nuclear Physics Group, STFC Daresbury Laboratory, Daresbury, United Kingdom
- 94 Nuclear Physics Institute of the Czech Academy of Sciences, Řež u Prahy, Czech Republic
- 95 Oak Ridge National Laboratory, Oak Ridge, TN, United States
- 96 Ohio State University, Columbus, OH, United States
- 97 Petersburg Nuclear Physics Institute, Gatchina, Russia
- 98 Physics Department, Faculty of Science, University of Zagreb, Zagreb, Croatia
- 99 Physics Department, Panjab University, Chandigarh, India
- 100 Physics Department, University of Jammu, Jammu, India
- 101 Physics Department, University of Rajasthan, Jaipur, India
- 102 Physikalisches Institut, Eberhard-Karls-Universität Tübingen, Tübingen, Germany
- 103 Physikalisches Institut, Ruprecht-Karls-Universität Heidelberg, Heidelberg, Germany
- 104 Physik Department, Technische Universität München, Munich, Germany
- 105 Politecnico di Bari, Bari, Italy
- 106 Research Division and ExtreMe Matter Institute EMMI, GSI Helmholtzzentrum für Schwerionenforschung GmbH, Darmstadt, Germany
- 107 Rudjer Bošković Institute, Zagreb, Croatia
- 108 Russian Federal Nuclear Center (VNIIEF), Sarov, Russia
- 109 Saha Institute of Nuclear Physics, Homi Bhabha National Institute, Kolkata, India
- 110 School of Physics and Astronomy, University of Birmingham, Birmingham, United Kingdom
- 111 Sección Física, Departamento de Ciencias, Pontificia Universidad Católica del Perú, Lima, Peru
- 112 St. Petersburg State University, St. Petersburg, Russia
- 113 Stefan Meyer Institut für Subatomare Physik (SMI), Vienna, Austria
- 114 SUBATECH, IMT Atlantique, Université de Nantes, CNRS-IN2P3, Nantes, France
- 115 Suranaree University of Technology, Nakhon Ratchasima, Thailand
- 116 Technical University of Košice, Košice, Slovakia
- 117 Technische Universität München, Excellence Cluster 'Universe', Munich, Germany
- 118 The Henryk Niewodniczanski Institute of Nuclear Physics, Polish Academy of Sciences, Cracow, Poland
- 119 The University of Texas at Austin, Austin, TX, United States
- 120 Universidad Autónoma de Sinaloa, Culiacán, Mexico
- 121 Universidade de São Paulo (USP), São Paulo, Brazil
- 122 Universidade Estadual de Campinas (UNICAMP), Campinas, Brazil
- 123 Universidade Federal do ABC, Santo Andre, Brazil
- 124 University of Cape Town, Cape Town, South Africa
- 125 University of Houston, Houston, TX, United States

- ¹²⁶ University of Jyväskylä, Jyväskylä, Finland
- ¹²⁷ University of Liverpool, Liverpool, United Kingdom
- ¹²⁸ University of Science and Technology of China, Hefei, China
- ¹²⁹ University of South-Eastern Norway, Tonsberg, Norway
- ¹³⁰ University of Tennessee, Knoxville, TN, United States
- ¹³¹ University of the Witwatersrand, Johannesburg, South Africa
- ¹³² University of Tokyo, Tokyo, Japan
- ¹³³ University of Tsukuba, Tsukuba, Japan
- ¹³⁴ Université Clermont Auvergne, CNRS/IN2P3, LPC, Clermont-Ferrand, France
- ¹³⁵ Université de Lyon, Université Lyon 1, CNRS/IN2P3, IPN-Lyon, Villeurbanne, Lyon, France
- ¹³⁶ Université de Strasbourg, CNRS, IPHC UMR 7178, F-67000 Strasbourg, France
- ¹³⁷ Université Paris-Saclay Centre d'Etudes de Saclay (CEA), IRFU, Département de Physique Nucléaire (DPn), Saclay, France
- ¹³⁸ Università degli Studi di Foggia, Foggia, Italy
- ¹³⁹ Università degli Studi di Pavia, Pavia, Italy
- ¹⁴⁰ Università di Brescia, Brescia, Italy
- ¹⁴¹ Variable Energy Cyclotron Centre, Homi Bhabha National Institute, Kolkata, India
- ¹⁴² Warsaw University of Technology, Warsaw, Poland
- ¹⁴³ Wayne State University, Detroit, MI, United States
- ¹⁴⁴ Westfälische Wilhelms-Universität Münster, Institut für Kernphysik, Münster, Germany
- ¹⁴⁵ Wigner Research Centre for Physics, Budapest, Hungary
- ¹⁴⁶ Yale University, New Haven, CT, United States
- ¹⁴⁷ Yonsei University, Seoul, Republic of Korea

ⁱ Deceased.

ⁱⁱ Dipartimento DET del Politecnico di Torino, Turin, Italy.

ⁱⁱⁱ M.V. Lomonosov Moscow State University, D.V. Skobeltsyn Institute of Nuclear Physics, Moscow, Russia.

^{iv} Department of Applied Physics, Aligarh Muslim University, Aligarh, India.

^v Institute of Theoretical Physics, University of Wrocław, Poland.